JCTC Journal of Chemical Theory and Computation

Multiconfiguration Molecular Mechanics Based on Combined Quantum Mechanical and Molecular Mechanical Calculations

Hai Lin,*[†,‡] Yan Zhao,[†] Oksana Tishchenko,[†] and Donald G. Truhlar*[†]

Chemistry Department and Supercomputing Institute, University of Minnesota, Minneapolis, Minnesota 55455-0431, and Chemistry Department, University of Colorado at Denver and Health Science Center, Denver, Colorado 80217-3364

Abstract: The multiconfiguration molecular mechanics (MCMM) method is a general algorithm for generating potential energy surfaces for chemical reactions by fitting high-level electronic structure data with the help of molecular mechanical (MM) potentials. It was previously developed as an extension of standard MM to reactive systems by inclusion of multidimensional resonance interactions between MM configurations corresponding to specific valence bonding patterns, with the resonance matrix element obtained from quantum mechanical (QM) electronic structure calculations. In particular, the resonance matrix element is obtained by multidimensional interpolation employing a finite number of geometries at which electronic-structure calculations of the energy, gradient, and Hessian are carried out. In this paper, we present a strategy for combining MCMM with hybrid quantum mechanical molecular mechanical (QM/MM) methods. In the new scheme, electronic-structure information for obtaining the resonance integral is obtained by means of hybrid QM/MM calculations instead of fully QM calculations. As such, the new strategy can be applied to the studies of very large reactive systems. The new MCMM scheme is tested for two hydrogen-transfer reactions. Very encouraging convergence is obtained for rate constants including tunneling, suggesting that the new MCMM method, called QM/MM-MCMM, is a very general, stable, and efficient procedure for generating potential energy surfaces for large reactive systems. The results are found to converge well with respect to the number of Hessians. The results are also compared to calculations in which the resonance integral data are obtained by pure QM, and this illustrates the sensitivity of reaction rate calculations to the treatment of the QM-MM border. For the smaller of the two systems, comparison is also made to direct dynamics calculations in which the potential energies are computed quantum mechanically on the fly.

1. Introduction

An accurate potential energy surface is an essential element in carrying out reliable dynamics simulations of a chemical reaction. Direct dynamics,[1−12] where the potential energy surface is calculated on the fly by electronic structure theory, is limited to relatively small systems or low levels of electronic structure theory due to the high computational costs of reliable electronic structure calculations. Multiconfiguration molecular mechanics (MCMM),[13−17] which is an extension of conventional molecular mechanics (MM)[18−47] so that it can be used for chemical reactions, is an alternative way to generate reactive potential energy surfaces with significantly reduced computational effort.

* Corresponding author fax: (612)624-9390; e-mail: truhlar@ umn.edu (D.G.T.); hai.lin@cudenver.edu (H.L.).
† University of Minnesota.
‡ University of Colorado at Denver and Heath Science Center.

In MCMM,[13-17] as in earlier semiempirical[48-55] and empirical[56-62] valence bond formulations, the actual representation for a system at a given geometry is obtained by mixing multiple (usually two: reactant and product) MM configurations; and as in empirical valence bond theory,[56-62] one constructs an electronically nonadiabatic (i.e., diabatic) Hamiltonian matrix **V** whose diagonal elements (V_{11} and V_{22}) are given by MM. The MM configuration of reactant (or product) is the bonding pattern for the system in the reactant (or product) state, and the corresponding energy is interpreted as a diagonal element of a valence bond configuration interaction Hamiltonian matrix. These valence bond states are also sometimes called diabatic electronic states. For example, in an atom transfer reaction AB + C → A + BC, the electronic wave function for any geometry can be considered to be composed of two interacting valence-bond or diabatic configurations (A−B, C) and (A, B−C), where "−" denotes a bond in MM and paired set of bonding orbitals in valence bond theory. Configuration interaction between the reactant and product configurations of different bonding patterns leads to the ground-state potential energy surface.

The resonance integral (V_{12}, which equals V_{21}) is the most critical element in MCMM, and it is at the heart of the MCMM methodology. In our implementation of MCMM,[13,14] the resonance integral is obtained by Shepard interpolation of quadratic expansions around a set of points where electronic structure data are available. The Born−Oppenheimer potential energy surface is approximated by the lowest eigenvalue of the matrix **V**, and the resonance integral reproduces a quadratic expansion[57] of the QM data in the vicinity of each electronic structure data point. This kind of nondiagonal representation of the Hamiltonian has been widely used in a variety of contexts for modeling reactive systems,[4,48-66] but in work prior to MCMM, the resonance integral was usually a simple functional form (even a constant) fit to one or more data and potential energy surface feature (e.g., barrier height) rather than, as in MCMM, a systematically improvable function fit to reproduce data at as many geometries as required to achieve convergence.

The MCMM approach not only is similar to the empirical valence-bond[56-62] (EVB) treatment but also contains critical differences.[13-15] (1) As mentioned in the previous paragraph, the resonance between valence-bond configurations is calibrated to the electronic-structure calculations instead of to often-limited kinetic data from experiments or accurate data only at the saddle point. (2) A very general scheme (the Shepard interpolation[67,68] scheme) is used to generate a semiglobal potential energy surface. In work reported so far and in the present article, the semiglobal surface is designed to be accurate in the kinetically important region for reaction-path rate calculations and large-curvature tunneling calculations (called the reaction swath,[7,69] i.e., the region near the reaction path including the region associated with small-curvature tunneling[7,70-74] and also the larger region on the concave side of the reaction valley that is critical for large-curvature tunneling[7,69,74-79]). In future work, MCMM will be extended to cover the entire region of the potential energy surface required to run classical trajectories.

The MCMM method can be considered to be a general and efficient fitting scheme for creating potential energy surfaces for reactive systems. A merit of the MCMM method is that it does not require the human judgment traditionally associated with the "art" of fitting multidimensional functions. The MCMM fitting process is unique and automatic, except for the choice of geometries to include, the choice of MM functions, and the choice of QM level. In principle the results converge to a numerically accurate interpolation of the potential energy surface for any reasonable scheme of adding data, although in practice one strategy of adding data points may converge the results faster than another strategy does. Moreover, MCMM does not require a uniform grid for adding data points; this flexibility of using a nonuniform distribution of data points allows one to obtain a fairly high accuracy from a reasonably small amount of electronic structure data by putting a dense set of data points in an interesting region, while a sparse set of data points is used in other regions and one can always improve the accuracy by including more data points whenever needed. Once constructed, the MCMM surface is inexpensive to calculate, with a cost roughly the same as conventional MM. Another notable merit of the MCMM method is that the constructed potential energy surface is full dimensional, since both the diagonal and off-diagonal elements in the diabatic Hamiltonian are full dimensional. The full-dimensional nature of the potential energy surface is critical for realistic modeling of chemical reactions.

An alternative approach is to restrict the functional form of the resonance matrix element and to obtain the parameters in the assumed functional form by global least-squares fitting.[59] This is a promising approach, but it is not systematically improvable like the MCMM algorithm based on Shepard interpolation. An alternative to straight Shepard interpolation that could be employed in MCMM is to combine it with interpolant moving least squares, as proposed by Ishida and Schatz.[80] In this method, one first performs local least-squares fitting with restricted functional forms (e.g., polynomials) for the energies from electronic-structure calculations at a set of given geometries, and one then computes the gradients and Hessians at these geometries by employing the locally fitted functions. Finally, one carries out Shepard interpolation based on these electronic-structure energies and approximate gradients and Hessians. This is a very promising method, because it maintains the merit of Shepard interpolation and avoids the electronic-structure calculations of gradients and Hessians, which are more expensive than for energies. However, we note that, as a tradeoff, this method requires a large amount of energetic data in order to ensure the approximated derivatives are accurate representations of the true (electronic-structure) derivatives. Whether one uses straight Shepard interpolation or an intermediate interpolant least squares step, the key feature that reduces the data requirements in MCMM is that one interpolates the relatively smooth V_{12} and combines it with powerful preexisting MM functions, whereas other work employing Shepard interpolation[67,68,81] interpolates the more structured ground-state potential energy surface and does not

Multiconfiguration Molecular Mechanics

J. Chem. Theory Comput., Vol. 2, No. 5, 2006 **1239**

take advantage of MM for the dependence of the potential on spectator degrees of freedom.

The usefulness of the MCMM scheme has been established for rate constant calculations as demonstrated by tests,[13,14,16,17,82] against a diverse set of reactions involving hydrogen transfer using variational transition state theory with multidimensional tunneling[7,73,74,79,83−86] (VTST/MT). It should be noted that the reactions used for tests are challenging ones, because of significant variational and tunneling effects. It is encouraging that a scheme involving predetermined locations for the points was able to predict rates in good agreement (∼10%) with direct dynamics for all reactions studied with only a dozen (or less) electronic-structure Hessians[13] or partial electronic-structure Hessians.[16]

As a fitting scheme for creating potential energy surfaces for reactive systems, the success of the MCMM method relies on the electronic-structure data at the Shepard input points. Electronic-structure calculations are feasible for small- and medium-size systems comprising tens to hundreds of atoms, depending on the level of theory involved. The partial electronic-structure Hessian scheme,[16] which uses electronic-structure calculated Hessian elements for active atoms and interpolated Hessian elements for spectator atoms for non-stationary Shepard points, reduces the computational cost by up to an order of magnitude, making it feasible to apply MCMM dynamics to large organic reactions. However, for even larger reactive systems such as enzymes, electronic-structure calculations are too expensive to be applied to the whole system, even just at the saddle point, and an alternative solution must be found.

Combined quantum mechanical and molecular mechanical (QM/MM) methods[87−145] are very promising as a practical way to extend electronic-structure calculations to large reactive systems where a reaction takes place in a localized region. (Extensions to cases where the localized region can change are also available.[95,110,132,145]) A QM/MM method treats this localized region, e.g., the active site and its neighbors in an enzyme (called the primary subsystem, PS), by a QM method and includes the influence of the surroundings (e.g., the protein and/or solvent environment, called the secondary subsystem, or SS) at the MM level. The QM/MM energy for the entire system (ES) can be formally defined by

$$E(QM/MM;ES) = E(QM;PS) + E(MM;SS) + E(QM/MM;PS|SS) \quad (1)$$

i.e., as a summation of the energy of the PS, the energy for the SS, and the interaction energy between them.

The PS is also called the QM subsystem, and the SS is often called the MM subsystem. The coupling between PS and SS can be treated either by mechanical embedding (ME) schemes,[92,103] where the electrostatic interaction is evaluated classically at the MM level, or by electrostatic embedding schemes[103,107] that describe the electrostatic interaction between the PS and SS as one-electron operators that enter the QM Hamiltonian. The interactions other than electrostatic, e.g., stretching, bending, torsion, and van der Waals interactions, are computed at the MM level in both mechanical embedding and electrostatic embedding schemes. Includ-
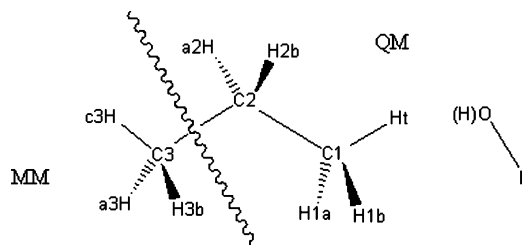

Figure 1. Reaction of OH with C_3H_8 to produce H_2O and CH_2-CH_2CH_3. The QM/MM boundary cuts through the C2−C3 bond.

ing the interactions between the active center and its environment allows a more realistic description of the system, in comparison with isolated QM calculations on subsystems, which are often called model systems. QM calculations on such model systems will be called cluster QM (CQM). Although the electronic structure for the surroundings does not change during the reaction (that is why we can use MM to describe it), the presence of the surroundings may affect the electronic structure of the active center (that is why we need to take it into account).

It therefore appears attractive to replace full QM calculations by QM/MM calculations in generating input data points for MCMM. This scheme can be called QM/MM-MCMM, and it will be the central topic of the present contribution. In comparison, the conventional MCMM scheme that is based on a full QM calculations can be called QM-MCMM or simply MCMM. Section II presents the QM/MM-MCMM scheme in detail.

The QM/MM and MCMM methods both represent ways to add QM elements to MM. The QM/MM method incorporates QM contributions based on size extension, while MCMM (or other valence-bond theories) builds in QM contributions vertically through interconfigurational resonance. Thus, the QM/MM-MCMM is a method that includes the QM contributions both laterally and vertically.

Another way to combine QM and MM both laterally and vertically can be called MCMM/MM or (QM-MCMM)/MM, where MCMM (also called QM-MCMM) is inserted into the QM part of the QM/MM methodology rather than, as in the present paper, inserting QM/MM into MCMM. (In other words, the MCMM surface describes only the primary system in MCMM/MM but describes the entire system in QM/MM-MCMM.) In MCMM/MM, one constructs an MCMM surface for the primary system based on QM/MM calculations for the entire system or based on CQM calculations on a model system, whichever is appropriate or practical, and uses this MCMM calculation to replace full QM calculations in subsequent QM/MM calculations. The MCMM/MM method may be useful in some circumstances where the interaction between the PS and SS can be well described at the MM level.

Our new QM/MM-MCMM method will be demonstrated by calculations on two H-transfer reactions. The first reaction, R1, which is illustrated in Figure 1, is the OH radical reacting with propane at the primary carbon; this reaction has been studied previously with the QM-MCMM scheme.[16] The second reaction, R2, is the OH radical reacting with camphor, as shown in Figure 2. In particular, we will compute the
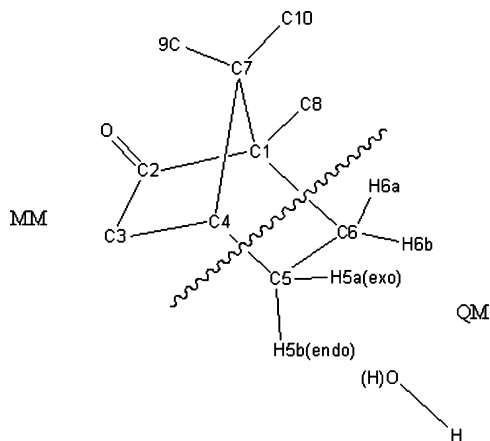
Figure 2. Reaction of OH with camphor. The QM/MM boundary cuts through the C4−C5 bond the C1−C6 bond. The hydrogen atoms are shown explicitly only in the QM region.

abstraction of the *exo*-hydrogen (H5a) at the C5 position. We note that the reaction of OH with camphor is important for atmospheric chemistry.[146−148] However, the reader should be aware that the reaction occurs along several pathways and does not occur with the greatest probability at the C5 carbon position.[147] One expects the H abstraction from a tertiary C−H bond at the C4 carbon position to have a larger rate than the abstraction from secondary and primary C−H bonds at the other carbon positions. Since the emphasis of the present study is to demonstrate the new QM/MM-MCMM methodology instead of to compare with experiment for the overall rate of reaction of OH with camphor (or to explain atmospheric chemistry), we selected the reaction at the C5 position because it is a better test for QM/MM.

The dynamics algorithm, calculations, and results will be presented in sections III, IV, and V, respectively, followed by a discussion of the results in section VI and concluding remarks in section VII.

II. The MCMM Algorithm Based on QM/MM Calculations

As explained in the Introduction, the QM/MM-MCMM method involves replacing full QM calculations by QM/MM calculations in generating input data points for MCMM. The QM-MCMM method was described in detail in ref 13. The QM/MM methodology used here and its implementation were also published previously.[143] Here, we only summarize briefly those aspects of MCMM and QM/MM related to the computations in this work, and we refer to the original references[13,143] for details.

II.A. QM-MCMM. MCMM approximates the Born−Oppenheimer potential energy at a geometry defined in internal coordinates $\mathbf{q}$ as the lowest eigenvalue of a 2×2 diabatic electronic Hamiltonian matrix $\mathbf{V}(\mathbf{q})$

$$\mathbf{V}(\mathbf{q}) = \begin{pmatrix} V_{11}(\mathbf{q}) & V_{12}(\mathbf{q}) \\ V_{12}(\mathbf{q}) & V_{22}(\mathbf{q}) \end{pmatrix} \tag{2}$$

where the V_{11} and V_{22} elements, as mentioned in the Introduction, are classical MM potential functions that describe the reactant and product valence bond configurations, and

the V_{12} matrix element is the resonance integral. In our implementation, the reactant (or product) configuration is the reactant well (or product well) valence bond configuration (for example, the reactant van der Waals complex of OH with propane or the product van der Waals complex of propyl radical with water). The lowest eigenvalue of eq 2 is

$$V(\mathbf{q}) = \frac{1}{2} \{ (V_{11}(\mathbf{q}) + V_{22}(\mathbf{q})) -$$
$$[(V_{11}(\mathbf{q}) - V_{22}(\mathbf{q}))^2 + 4V_{12}(\mathbf{q})^2]^{1/2} \} \tag{3}$$

The potential energy surface $V(\mathbf{q})$, and its first and second derivatives, which are required for the dynamical calculations, are obtained by analytic differentiation of eq 3 after we know $V_{11}(\mathbf{q})$, $V_{22}(\mathbf{q})$, and $V_{12}(\mathbf{q})$. The terms associated with $V_{11}(\mathbf{q})$ and $V_{22}(\mathbf{q})$ are readily available from MM calculations, and the central problem is how to obtain the resonance integral $V_{12}(\mathbf{q})$ and its derivatives.

The construction of $V_{12}(\mathbf{q})$ is carried out in two steps. First, at a number of selected geometries $\mathbf{q}^{(k)}$, with $k = 1, 2, ...,$ M, one computes the energies $V(\mathbf{q}^{(k)})$, gradients $\mathbf{g}^{(k)}$, and Hessian matrices $\mathbf{f}^{(k)}$ by electronic-structure calculations, and one evaluates $V_{12}(\mathbf{q};k)$ and its derivatives by using eq 2 inversely thereafter, i.e., evaluates $V_{12}(\mathbf{q};k)$ from $V_{11}(\mathbf{q};k)$, $V_{22}(\mathbf{q};k)$, and $V(\mathbf{q};k)$.[57] The set of M data points $\mathbf{q}^{(k)}$ are called Shepard points. Second, based on this set of M data points of $V_{12}(\mathbf{q};k)$, V_{12} at a desired geometry $\mathbf{q}$ can be evaluated by Shepard interpolation[67,68,81] as a linear combination of the quadratic expansions around these Shepard points

$$V_{12}^S(\mathbf{q}) = \sum_{k=1}^{M} W_k(\mathbf{q}) V_{12}^{mod}(\mathbf{q};k) \tag{4}$$

where $W_k(\mathbf{q})$ are normalized weights, and $V_{12}^{mod}(\mathbf{q};k)$ is a modified quadratic function, as defined in ref 13. Once the interpolation is constructed, $V_{12}(\mathbf{q})$ and its derivatives are available analytically at any desired geometry, and one can calculate $V(\mathbf{q})$ according to eq 4.

Because the MCMM representation of the potential surface is based on both electronic structure calculations and MM energies, and because the latter have different zeros of energy at reactant and product configurations, a unique energy scale must be defined across the potential energy surface. We use the same procedure here as in previous work.[166] In particular, we define the zero of energy to be the electronic structure theory energy at the MM equilibrium geometry corresponding to the reactant valence bond configuration (where the two reactants are infinitely far apart in the case of a bimolecular reaction), and we adjust the MM energies for V_{11} and V_{22} as follows

$$V_{11} = V_{11}^{MM} - V_o(I) \tag{5}$$

$$V_{22} = V_{22}^{MM} - V_o(II) + \Delta E \tag{6}$$

where $V_o(I)$ and $V_o(II)$ are MM energies at the MM equilibrium geometries corresponding to valence bond configurations I (where the two reactants are infinitely far apart in the case of a bimolecular reaction) and II (where the two products are infinitely far apart in the case of two products), and ΔE is the electronic-structure theory energy of the product relative to the reactant.

Multiconfiguration Molecular Mechanics

J. Chem. Theory Comput., Vol. 2, No. 5, 2006 **1241**

As one can see from the above procedure, the accuracy of an MCMM surface depends on the accuracy of the Shepard data points obtained by QM or QM/MM calculations and used as input. In principle the results converge to a numerically accurate interpolation of the potential energy surface with the inclusion of more Shepard points. In practical applications, one wishes to limit the computational cost by using only a small number of data points. We have proposed and tested a general scheme[14] where only one to ten electronic-structure points, including the saddle point and 0−9 nonstationary points, are needed to generate a potential energy that produces reasonably accurate rate constants in the VTST/MT calculations.[14,82] We also demonstrated that, when several Hessians were required in the original scheme, the efficiency of this scheme could be significantly improved up to a factor of 11 by employing partial electronic-structure Hessians.[16] We emphasize that this scheme might not be the best scheme for a specific reaction,[17] but it was found to be applicable to a diverse set of reactions, and it provides a start from which future refinement can be performed.

II.B. QM/MM. As mentioned in the Introduction, the QM/MM method can be viewed as a generalized electronic-structure method for large reactive systems where reaction takes place in a localized region (the primary system, PS). The PS is described at the QM level, and its environment (the secondary subsystem, SS) is treated at the MM level. The electrostatic interaction between PS and SS is either calculated classically at the MM level in the mechanical embedding schemes[92,103,144] or modeled as one-electron operators that enter the QM Hamiltonian in the electrostatic embedding schemes.[103,107,144] The interactions other than electrostatic interaction between the PS and the SS are computed at the MM level in both the mechanical embedding and electrostatic embedding schemes.

A question arises in QM/MM calculations: how should one select MM parameters for the PS atoms in calculation of the coupling between PS and SS atoms? These MM parameters are not necessarily the same for the PS atoms in the reactant and product because the atom types are changed for some atoms, e.g., a carbon atom may change from C=O type to C−O−H type. This will particularly be a concern if the boundary between the PS and the SS is very close to the active site. An extensive discussion has been given in our recent review,[144] and here we note that there is no unambiguous answer. Our suggestion is to use one set of MM parameters and to examine whether the errors introduced by using one set of parameters exceed the errors produced by other approximations that are introduced by the QM/MM framework. Although our treatment is not a perfect solution, it is very practical, and it appears to be reasonable.[143] Note that this problem occurs for QM/MM but not for MCMM. (In the present study we used the product parameters; therefore, we need parameters for a carbon radical atom type. See the Supporting Information for details.)

Another important issue in QM/MM is how to treat the dangling bonds of the PS when a QM/MM boundary cuts through covalent bonds. Various schemes have been developed to handle such a situation. Those schemes differ from each other mainly in two aspects: (i) how to treat the degrees of freedom of the nuclei of the SS atoms that are directly bond to the PS atoms and (ii) how to treat the charge distribution at the boundary. The charge distribution at the boundary is simply ignored in the mechanical embedding scheme, and its inclusion in the electrostatic embedding schemes is the major source of differences among these schemes. Our treatment[143] of the first aspect, following others,[88,89] is to saturate the dangling bond at the PS by a normal hydrogen atom (the so-called hydrogen-link atom, HL). The coordinates of HL are determined as a linear combination of the coordinates of the PS and SS boundary atoms between which the covalent bond is cut. More precisely, we place the HL atom on the Q1−M1 bond, where the Q1 and M1 denote the PS and SS boundary atoms, respectively. We scale the Q1−HL distance $R(\text{Q1-HL})$ with respect to the Q1−M1 distance $R(\text{Q1−M1})$ by a scaling factor C_{HL}, in the same way as proposed by Morokuma and co-workers[99,120]

$$R(\text{Q1−HL}) = C_{\text{HL}}R(\text{Q1−M1}) \tag{7}$$

$$C_{\text{HL}} = R_0(\text{Q1−H})/R_0(\text{Q1−M1}) \tag{8}$$

where $R_0(\text{Q1−H})$ and $R_0(\text{Q1−M1})$ are the MM bond distance parameters for the Q1−H and Q1−M1 stretches, respectively, in the employed MM force field. Such a treatment eliminates the extra degrees of freedom due to the artificially introduced link atoms, making dynamics calculations meaningful.

It is important to retain a qualitatively correct charge distribution near the QM/MM boundary, especially when there are MM atoms carrying substantial partial charges close to the boundary, as demonstrated in a recent publication.[143] Such a situation motivates one to use an electrostatic embedding scheme, which allows the electronic structure of the PS to respond to the presence of the charge distribution of the SS. Here we use our recently developed redistributed charge and dipole (RCD) scheme[143] as the electrostatic embedding scheme. The RCD scheme for electrostatic embedding involves distributing the M1 charge evenly onto midpoints of the M1−M2 bonds, where M2 is an SS atom that directly bonds to the M1 atom, and further modifies both the redistributed charges and the charges on the M2 atoms in order to preserve the M1−M2 bond dipoles. For example, suppose that there are n M2 atoms bonded to the M1 atom and that the charges on the M1 and M2 atoms are q_{M1} and $q_{\text{M2},k}$ ($k = 1, 2, ..., n$), respectively. The initially redistributed charge q_0 is determined by

$$q_0 = q_{\text{M1}/n} \tag{9}$$

and the final redistributed charge q_0^{RCD} is given by

$$q_0^{\text{RCD}} = 2q_0 \tag{10}$$

and the modified M2 charges $q_{\text{M2},k}^{\text{RCD}}$ are

$$q_{\text{M2},k}^{\text{RCD}} = q_{\text{M2},k} - q_0 \tag{11}$$

The QM calculations are carried out in the presence of the redistributed charges and the charges on the SS atoms.

The QM/MM gradient and Hessians are calculated by use of the chain rule, as described in refs 99 and 120.

II.C. QM/MM-MCMM. QM/MM-MCMM differs from QM-MCMM in the use of QM/MM calculations instead of QM calculations to provide energies, gradients, and Hessians at the Shepard points. A central concern in such a replacement of QM calculations by QM/MM calculations is how accurately the QM/MM description approximates the QM one or, since the QM one is itself approximate, how accurate QM/MM is in comparison to experiment. Attention should be paid to various issues. The first is how much the geometries and energies will change, e.g., at the stationary points of the potential energy surface. If used with care, QM/MM calculations may produce reasonably accurate geometric and energetic data in comparison with full QM calculations. Due to its intrinsic limitations, e.g., the prohibition of charge transfer between PS and SS, the QM/MM method is not designed to give the highest possible quantitative accuracy. It is probably more useful to stress the qualitative conclusions, and, when quantitative comparisons are made, one should focus on relative energies where the errors may cancel to some extent.

The second issue is the Hessian, which determines the vibrational frequencies and their associated eigenvectors. The QM and QM/MM Hessians usually show substantial differences, due to the different QM and MM frequencies as well as the additional approximation at the boundary. This is especially a concern for modes that involve simultaneous motions of both PS and SS atoms. This makes precise correlation of QM modes with QM/MM modes ambiguous. Visualization of the vibrations helps to some extent, but its use is limited if the system is big. Thus, a one-to-one comparison between the QM, MM, and QM/MM vibrational modes is only approximate.

The vibrational frequencies are important for determination of the zero-point vibrational energies and the vibrational partition functions. In many cases, the deviations of the QM/MM frequencies from the QM frequencies are similar for the reactant state, at the saddle point, at the product, and along the reaction path that connects these three geometries. Since it is often the relative zero-point energy rather than the absolute zero-point energy that matters, the systematic underestimation or overestimation of the frequencies in QM/MM computations can lead to at least partial cancellation of errors. The error cancellation is, however, less complete for the low-frequency modes, for which the harmonic partition functions are very sensitive to the change of frequencies. One should take this into consideration when assessing the performance of any rate calculation employing the harmonic approximation.

The eigenvector of the imaginary-frequency mode at the saddle point, which is often highly localized and is easily characterized, is used in determination of the reaction path. Usually, this imaginary-frequency mode involves motions of the PS atoms at or close to the reaction center, and its eigenvector is often very similar in the QM and QM/MM calculations.

The eigenvectors of the generalized normal mode vibrational modes along the reaction path are also important in determination of the coupling between the motion of reaction coordinate and the spectator coordinates. Such coupling plays a critical role in certain types of calculations, e.g., tunneling calculations. One needs considerably more experience testing QM/MM calculations to assess their performance for such detailed dynamical issues.

III. Dynamics

The dynamics calculations in this work were carried out in the framework of VTST/MT,[73,74,79,83−86] whose validity has been well-established.[149−151] The conventional transition state theory (TST) rate constants were determined by

$$k^{\text{TST}} = (\sigma/\beta h)(Q^{\ddagger}/\Phi^{R}) \exp(-\beta V^{\ddagger}) \qquad (12)$$

where σ is the symmetry factor that represents the reaction path multiplicity, i.e., the number of equivalent reaction paths from reactant to product, and σ is 1 for the reactions in this work, $\beta = k_{\text{B}}T$, k_{B} is Boltzmann's constant, T is the temperature, h is Planck's constant, $Q^{\ddagger}$ is the generalized partition functions for the system at the saddle point, Φ^{R} is the partition function per unit volume of the reactant, and $V^{\ddagger}$ is the classical barrier height. The generalized partition function is a product of partition functions for electronic, vibrational, and rotational degrees of freedom as well as, for bimolecular reactions, the relative translational partition function per unit volume:

$$Q(s,T) = Q_{\text{el}}(s,T)Q_{\text{vib}}(s,T)Q_{\text{rot}}(s,T) \qquad (13)$$

$$\Phi^{R}(T) = \Phi^{R}_{\text{el}}(T)\Phi^{R}_{\text{vib}}(T)\Phi^{R}_{\text{rot}}(T)\Phi^{R}_{\text{rel}}(T) \qquad (14)$$

Here s is the signed distance from the saddle point along the minimum energy path (MEP) in mass-scaled coordinates,[152] where $s = 0$ corresponds to the saddle point.

The canonical variational transition state (CVT) rate constants were computed by

$$k^{\text{CVT}} = (\sigma/\beta h)(Q^{\text{CVT}}/\Phi^{R})\exp[-\beta V_{\text{MEP}}(s^*)] \qquad (15)$$

where Q^{CVT} is the generalized total partition function at the CVT bottleneck location s^* on the reaction path, $V_{\text{MEP}}(s^*)$ is the potential energy on $V_{\text{MEP}}(s)$ at s^*, and $V_{\text{MEP}}(s)$ is the potential energy along the MEP. The CVT bottleneck location, s^*, is the place on the reaction path where the generalized free energy of activation is a maximum.[84]

We considered two kinds of tunneling calculations, both of which involve the vibrationally adiabatic ground-state potential energy curve, which is expressed as

$$V_{\text{a}}^{\text{G}}(s) = V_{\text{MEP}}(s) + \sum_{m=1}^{3N-7} \epsilon_{m}^{\text{G}}(s) \qquad (16)$$

where N is the total number of atoms in the system, m denotes a generalized normal-mode vibration transverse to the reaction coordinate, and $\epsilon_{m}^{G}(s)$ is the zero-point energy of these generalized normal-mode vibrations at s. The maximum of $V_{\text{a}}^{\text{G}}(s)$ is called V_{a}^{AG}. The first kind of tunneling calculations is the small-curvature tunneling (SCT) ap-

Multiconfiguration Molecular Mechanics

J. Chem. Theory Comput., Vol. 2, No. 5, 2006 **1243**

proximation,[73,74] which calculates the transmission coefficients semiclassically including the effects of reaction-path curvature,[70,72,83,84,152−155] which enters the calculations through an effective mass[73,74] for the reaction-path motion. The second type of tunneling contribution is the large-curvature tunneling (LCT)[74,79,86] approximation, which assumes that tunneling occurs along the most direct path between the reactant and product valleys in the potential energy surface without necessarily assuming vibrational adiabaticity relative to the reaction-coordinate motion. The LCT calculations include tunneling into vibrationally excited diabatic vibrational states. In direct dynamics calculations, excited states are included to the extent that they contribute; however, in MCMM we include up to the vibrational quantum number of the highest excited state determined by a prespecified protocol. In this protocol,[16] the highest vibrational quantum number is increased successively until the tunneling contribution is converged within 1% or until the contribution from the newly added state reaches a local minimum (with respect to vibrational quantum number), whichever happens first. Such a prespecified protocol for the determination of how many final states to include in the LCT calculation has been shown[16] to be helpful in avoiding artificially large tunneling rates in MCMM dynamics due to the possibly inaccurate potential energy surface far away from the reaction swath where Shepard points are missing. In analyzing the results it is often useful to also consider the LCT(0) approximation, which includes tunneling only into the ground vibrationally diabatic state. The final best tunneling approximation is microcanonically optimized multidimensional tunneling (μOMT), which is obtained by accepting the larger of the SCT and LCT results at each tunneling energy.[86] All LCT and LCT(0) calculations in this paper were carried out with the version 4[79] algorithm.

A special note is made for the calculations of vibrational partition functions of the low-frequency modes. An accurate calculation of thermodynamic functions for these low-frequency modes is, generally speaking, very challenging. Such low-frequency modes are often associated with large-amplitude motions, and the routinely used harmonic approximation is suspicious for the evaluation of vibrational partition functions for these modes. For modes of very low frequencies (<10 cm^{-1}), the use of harmonic approximation can be qualitatively incorrect and lead to large errors. However, an accurate and effective approach to include the anharmonicity is yet to be developed. Therefore, we make a compromise in this work by use of the harmonic approximation for all vibrational modes with a cutoff frequency in the thermodynamic calculations, i.e., whenever the frequency of a mode is smaller than the prespecified (cutoff) frequency, the cutoff frequency will be used instead in calculations of vibrational partition functions. This procedure of using a cutoff frequency has been adopted[16] in our previous studies. Although one cannot expect very high accuracy from such a crude treatment, it is hoped that this procedure may provide a more realistic estimation of the vibrational partition functions than simply using the calculated harmonic frequency.

IV. Calculations

IV.A. QM Calculations. The first reaction (R1) was studied recently (as reaction R6 in ref 16) by direct dynamics and by QM-MCMM dynamics employing QM calculations at the MPW1K/6-31+G(d,p) level in generation of a potential energy surface. Briefly, the modified Perdew-Wang 1-parameter model for kinetics (MPW1K)[156,157] is a hybrid Hartree−Fock density functional theory (HF-DFT) model, whose parameters had been optimized against a selected database that consists of 20 forward barrier heights (BHs), 20 reverse BHs, and 20 energies of reaction. The one-parameter hybrid Fock-Kohn−Sham operator can be written as follows

$$F = F^{\text{H}} + (X/100)F^{\text{HFE}} + [1 - (X/100)](F^{\text{SE}} + F^{\text{GCE}}) + F^{\text{C}} \tag{17}$$

where F^{H} is the Hartree operator, F^{HFE} is the Hartree−Fock exchange operator, X is the percentage of HF exchange, F^{SE} is the Dirac−Slater local density functional for exchange, F^{GCE} is the gradient corrections for the exchange functional, and F^{C} is the total correlation functional including both local and gradient-corrected parts. The MPW1K model uses the Adamo and Barone's modified Perdew-Wang 1991 exchange functional (mPW)[158] for F^{GCE} and Perdew and Wang's 1991 correlation functional (PW91)[159] for F^{C}, and set $X = 42.8$. The 6-31+G(d,p)[160] basis set is also denoted as the DIDZ basis set in this paper.

For the second reaction (R2), we used the newly developed MPWB1K[161] density function and again the 6-31+G(d,p) basis set. The MPWB1K model is very similar to the MPW1K model, but it uses the Becke95 functional[162] for F^{C}, and X was adjusted to 44. The calculations were carried out by use of the *Gaussian03* package.[163]

IV.B. MM Calculations. The MM calculations were performed by use of a locally modified TINKER program.[164] For reaction R1, the MM3 force field[20−22] was selected for both the QM/MM and MCMM calculations, and the same force field parameters as used in the previous studies[14,16] were employed, so that the results are comparable with the previous ones.

For reaction R2, the CHARMM27 force field[37] was selected for the QM/MM calculations, and the MM3 force field (modified as discussed below) was used for the MCMM calculations. This illustrates that the QM/MM calculation and the MM calculation that are combined by the MCMM scheme need not be related to one another in any special way.

Note that for the reaction R2, CHARMM27 is the same as CHARMM22. The CHARMM27 force field used for the QM/MM calculations needs to be augmented by a set of parameters for atom types (e.g., carbon radical) that are not defined in the standard CHARMM27 force field. These augmented MM parameters were set to the parameters for similar atom types, with adjustment of the point charges to maintain the neutrality of the camphor and camphor radical species. The point charges for the OH radical are obtained in a different manner, i.e., they are derived using the Merz−Singh−Kollmann[88,165] electrostatic potential (ESP) fitting procedure from electronic-structure calculations for the OH

1244 *J. Chem. Theory Comput., Vol. 2, No. 5, 2006*

Lin et al.

radical at the MPWB1K/DIDZ level. We assume that the final results are not especially sensitive to these parameter choices, and we are satisfied if the selected MM parameters provide a qualitatively corrected zero-order description of the system.

A detailed description of the CHARMM parameters used here is given in Table S1 of the Supporting Information. These MM parameters are validated by comparisons between MM- and QM-optimized geometries of the reactant and product. Reasonably good agreement between the MM and QM results is achieved, as demonstrated in Table S2 in the Supporting Information, indicating that the augmented MM parameters are appropriate.

As mentioned above, the MM3 force field used for reaction R2 was modified. In particular, we use the MM3[20−22] parametrization with one exception. In MM3 the van der Waals interaction is given by the Buckingham Exp-6 potential

$$V_{\text{Exp}-6}(r) = \epsilon\left[Ae^{-Br/r_o} - C\left(\frac{r_o}{r}\right)^6\right] \qquad (18)$$

where r_o is the sum of the van der Waals radii, and ϵ is the energy parameter for the interaction between two atoms. The van der Waals term in the MC-TINKER program[166] that we have used in previous work for MCMM calculations is written as a linear combination of eq 18 and an r^{-12} term that represents repulsion

$$E_{\text{vdw}}(r) = \epsilon\left[Ae^{Br/r_o} - C\left(\frac{r_o}{r}\right)^6 + D\alpha\left(\frac{r_o}{r}\right)^{12}\right] \qquad (19)$$

where α is defined as

$$\alpha = \frac{V_{\text{Exp}-6}(r)}{\epsilon((r_o/r))^{12}}\bigg|_{r=(1/2)r_o} \qquad (20)$$

which yields

$$\alpha = [Ae^{-1/2} - C(2.0)^6]/2.0^{12} \qquad (21)$$

The values for the unitless parameters A, B, and C are the same as in the original MM3 formulation,[20] viz. 184 000.0, 12.0, and 2.25, respectively. In the original version of MC-TINKER, D was arbitrarily set to 0.2. However, a better value is usually in the range 0.005−0.02. We found that the optimum value for D for the camphor reactions is 0.01. The optimum value is found by running a few MCMM(0) calculations with values of D in the range 0.005−0.2 and selecting the one that gives the most realistic contour map. For reaction R1, we used the original MC-TINKER value of 0.2.

IV.C. QM/MM Calculations. The QM/MM calculations were performed by use of the QMMM program,[167] which calls a QM package and an MM package to perform the required single-level calculations and then combines the single-level calculations into multilevel results. In this work, the QM package *Gaussian03*[163] and the MM program TINKER[164] are called. Geometry optimizations were carried out using the optimizer[168] in *Gaussian03* through the *external* option available in *Gausian03*.

The partitioning of the systems into PS (QM) and SS (MM) regions is shown in Figure 1 for reaction R1 and in Figure 2 for reaction R2. The QM/MM boundary cuts through one C−C bond in R1 and two C−C bonds in R2. The PSs capped by the hydrogen-link atoms in both reactions are the same, i.e., OH + C_2H_6. The mechanical embedding scheme was selected for R1, and the RCD electrostatic embedding scheme described in section II.B was chosen for R2. The MPW1K/6-31+G(d,p) and MPWB1K/6-31+G(d,p) levels were selected for R1 and R2, respectively, being the same as those in pure QM calculations. Also, the same MM parameters were employed as those used in the pure MM calculations, i.e., MM3 for R1 and CHARMM27 for R2. One motivation to use different QM methods, different MM force fields, and different embedding schemes for these two reactions is to demonstrate the generality of the QM/MM-MCMM algorithm as well as the capacity of the programs in handling a diversity of QM, MM, and QM/MM methods. Note that the QM/MM calculations do not require special/extra parametrization for the given QM level of theory and/or for the given MM force field.

IV.D. Direct Dynamics Calculations. The direct dynamics calculations for reaction R1 have been reported previously by use of the GAUSSRATE program,[169] and we reran the calculations by using a different cutoff frequency in evaluation of the thermodynamic functions. The current cutoff frequency is set to 50 cm^{-1}, and it is larger than the previous cutoff frequency (10 cm^{-1}),[16] which we think is too conservative. Due to the very high computational cost, we did not carry out direct dynamics calculations for reaction R2.

IV.E. QM-MCMM Dynamics Calculations. The QM-MCMM dynamics calculations for reaction R1 have been reported previously[16] employing a cutoff frequency of 10 cm^{-1} in evaluation of the thermodynamic functions. In the current study, we reran the calculations by using a different cutoff frequency of 50 cm^{-1}. In calculating statistical mechanical quantities such as partition functions and free energies, any frequency below the cutoff is increased to the cutoff value as a way to account, very approximately, for anharmonic effects on low-frequency vibrations. (Often, for H transfer reactions, there is one low frequency near the saddle point, although when one extends the reaction path to large |s|, there are others because some frequencies transform to orbital-rotational motions.)

The QM-MCMM dynamics calculations for reaction R2 were performed following the same well-established procedure[14] as that used in the calculations for reaction R1. Briefly, one begins dynamics calculations with an MCMM potential energy surface that is Shepard-interpolated on the basis of three stationary points (the reactant well, the product well, and the saddle point), and one successively adds up to 10 nonstationary points (seven in the valley of MEP and three in the concave-side region that is important for LCT computations) to improve the accuracy of the MCMM potential energy surface. Dynamics calculations based on the 3 stationary and n ($n = 0, 1, ..., 10$) nonstationary points are called MCMM−n dynamics calculations, and the MCMM-10 results are the final result that are reported in this work.

Multiconfiguration Molecular Mechanics

J. Chem. Theory Comput., Vol. 2, No. 5, 2006 **1245**

More details about how to locate the nonstationary points have been given in ref 14 and summarized in Table S1 (Supporting Information) in ref 16, and they are not repeated here.

The Page−McIver[170] method was chosen to follow the MEP in mass-scaled coordinates, which were scaled to a reduced mass μ of 1 amu. A step size of 0.001 a_0 was used for the gradient, and a new Hessian was calculated every 0.01 a_0 along the MEP. The reaction path was calculated out to $s = -3.0$ a_0 on the reactant side and to $s = 2.0$ $a0$ on the product side. We included the electronically excited $^2\Pi_{1/2}$ state of OH with an excitation energy of 140 cm^{-1} in calculating the reactant partition functions. The generalized normal-mode analyses were carried out using redundant internal coordinates; in particular, for reaction R1, we use the same redundant internal coordinates as used in our previously study,[16] and for reaction R2, we use the set of internal coordinates listed in Table S3 in the Supporting Information. The harmonic approximation was employed for all modes. A cutoff frequency of 50 cm^{-1} was selected for computing vibrational partition functions (that is, all frequencies below 50 cm^{-1} were replaced by the value of 50 cm^{-1} to simulate anharmonicity in low-frequency modes).

The QM-MCMM dynamics calculations were carried out by use of the MC-TINKERATE program.[171]

IV.F. QM/MM-MCMM Dynamics Calculations. The QM/MM-MCMM dynamics calculations for both reactions were carried out following the same procedure as the one used for the QM-MCMM dynamics calculations (see Section IV.E). The same setting was also used for following the MEP and for computing thermodynamic functions. The QM/MM-MCMM dynamics calculations were carried out by use of the MC-TINKERATE program.[171]

V. Results

The energetic and saddle-point geometric data are collected in Table 1. The QM data for reaction R1 have been reported previously, and they are tabulated here for comparison. A statistical summary of the comparison between QM and QM/MM vibrational frequencies is listed in Table 2, while the frequencies are given in Table S4 for reaction R1 and Table S5 for reaction R2 in the Supporting Information. In Table 3, we compare the locations of the first 7 nonstationary points in the QM-MCMM and QM/MM-MCMM dynamics calculations for reaction R1, the locations being indicated by the value of s, the signed distance from the saddle point along the MEP. The reaction-path curvature, κ, is illustrated as a function of s along the MEP for reaction R1 in Figure 3. The convergence of the rate constants with respect to the number of nonstationary Hessians is shown in Tables 4 and 5. After this all MCMM results shown in the article (in subsequent tables) are the final MCMM-10 ones.

The rate constants for reactions R1 and R2 are presented in Tables 6 and 7, respectively; Table 8 shows the percentage error for the rate constants of R1 calculated by the QM-MCMM dynamics and by the QM/MM-MCMM dynamics

Table 1. Reaction Energies, Barrier Heights, Saddle Point Geometries, and the Vibrational Imaginary Frequency at the Saddle Point for the Reactions OH + Propane (R1) and OH + Camphor (R2)^a

	QM	QM/MM	CPS
		R1^b	
ΔE	−12.6	−13.2	−13.1
$V^{\ddagger}$	4.9	4.7	3.9
$R_{O(H)-Ht}$	1.337	1.343	1.343
R_{C1-Ht}	1.195	1.191	1.192
$\theta_{C1-Ht-O(H)}$	177.2	178.2	177.7
$\omega^{\ddagger}$	1004i	958i	969i
		R2^c	
ΔE	−16.3	−14.0	−13.1
$V^{\ddagger d}$	1.8	2.9	3.9
$R_{O(H)-H5a}{}^d$	1.392	1.337	1.347
$R_{C5-H5a}{}^d$	1.173	1.198	1.190
$\theta_{C5-H5a-O(H)}{}^d$	172.6	167.8	178.1
$\omega^{\ddagger d}$	538i	966i	861i

^{a} Energy in kcal/mol, distance in Å, angles in degree, and frequency in cm^{-1}. The capped primary system (CPS) is OH + C_2H_6 for both reactions. ^{b} Reaction takes place at the C1 position. The MPW1K/DIDZ level of theory is used in QM calculations, and the MM3 force field is used for MM calculations. See Figure 1 for the QM/MM boundary setup. The mechanical embedding scheme was used in QM/MM computations. ^{c} The MPWB1K/DIDZ level of theory in QM calculations and CHARMM27 force field for MM calculations. See Table S1 in the Supporting Information for augmented MM parameters. See Figure 2 for the QM/MM boundary setup. The electrostatic embedding (EE) scheme redistributed charge and dipole (RCD) was used in QM/MM computations. ^{d} Abstraction of *exo* H5a.

with respect to those calculated by direct dynamics. Listed in Table 9 are the percentage errors for the rate constants of R2 calculated by QM/MM-MCMM dynamics with respect to QM-MCMM. In general, a percentage deviation is calculated as

$$PD = \frac{y^{Cal} - y^{Std}}{y^{Std}} \times 100\% \quad (22)$$

where y^{Cal} is the quantity to be examined (e.g., rate constants calculated by MCMM dynamics), and y^{Std} is the standard result (e.g., rate constants calculated by direct dynamics) that the calculation tries to reproduce.

For an assessment of the overall performance of the calculations, we calculated the mean signed deviation (MSD) and mean unsigned deviation (MUD) for a set of quantities as follows

$$MSD = \frac{1}{N} \sum_{i=1}^{N} (y_i^{Cal} - y_i^{Std}) \quad (23)$$

$$MUD = \frac{1}{N} \sum_{i=1}^{N} |y_i^{Cal} - y_i^{Std}| \quad (24)$$

where y_i^{Cal} is the quantity to be examined, y_i^{Std} is the standard result that the calculation tries to reproduce, and N is the number of quantities for which the comparisons are made.

Table 2. Statistic Summary of the Deviations between the QM and the QM/MM Vibrational Frequencies for the Reactions OH + Propane (R1) and OH + Camphor (R2)[a]

	reactant	product	saddle point	
R1[b]				
num. of modes				
total	27	24	32	
$|\Delta\nu| > 100$ cm^{-1}	3	3	3	
$|\Delta\nu| < 10$ cm^{-1}	11	5	14	
MSD[c] [cm^{-1}]	−32	−35	−26	
MUD[d] [cm^{-1}]	39	50	34	
$|\Delta\nu|_{max}$ [cm^{-1}]	244	247	249	
R2[e]				
num. of modes				
total	75	72	80[f]	
$|\Delta\nu| > 100$ cm^{-1}	13	13	13[d]	13[e]
$|\Delta\nu| < 10$ cm^{-1}	11	9	8[d]	14[e]
MSD[c] [cm^{-1}]	−61	−62	−62[d]	−61[e]
MUD[d] [cm^{-1}]	67	72	71[d]	71[e]
$|\Delta\nu|_{max}$ [cm^{-1}]	332	374	352[d]	360[e]

[a] Frequency in cm^{-1}. The deviation is calculated as $\Delta\nu = (\nu_{QM/MM} - \nu_{QM})$, where the modes are arranged in order of decreasing magnitude. The OH and H$_2$O species are always treated at the pure QM level, and they are not included in the comparisons. The imaginary-frequency mode has been shown in Table 1, and it is excluded from the comparison in this table. [b] Reaction takes place at the C1 position. The MPW1K/DIDZ level of theory is used in QM calculations, and the MM3 force field is used for MM calculations. See Figure 1 for the QM/MM boundary setup. The mechanical embedding (ME) scheme was used in QM/MM computations. [c] Defined by eq 21. [d] Defined by eq 22. [e] The MPWB1K/DIDZ level of theory in QM calculations and CHARMM27 force field for MM calculations. See Table S1 in the Supporting Information for augmented MM parameters. See Figure 2 for the QM/MM boundary setup. The electrostatic embedding (EE) scheme redistributed charge and dipole (RCD) was used in QM/MM computations. [f] Abstraction of *exo* H5a.

The mean signed percentage deviation (MSPD) and mean unsigned percentage deviation (MUPD) are defined in a manner similar to the MSD and MUD

$$\text{MSPD} = \left(\frac{1}{N}\sum_{i=1}^{N}\frac{y_i^{Cal} - y_i^{Std}}{y_i^{Std}}\right) \times 100\% \qquad (25)$$

$$\text{MUPD} = \left(\frac{1}{N}\sum_{i=1}^{N}\left|\frac{y_i^{Cal} - y_i^{Std}}{y_i^{Std}}\right|\right) \times 100\% \qquad (26)$$

Obviously, the MSPD and MUPD do not give an even-handed representation of the cases in which the quantities are underestimated (those cases are limited to a percentage error of 100%); however, they are still very instructive.

VI. Discussion

As can be seen Table 1, the QM/MM computations reproduce the QM barrier heights and reaction energies reasonably well, and the QM/MM results outperform the capped primary system (CPS) studies at the same QM level considerably. For reaction R1, the QM/MM barrier height is only 0.2 kcal/mol lower than the QM barrier height. The good agreement in energetics leads to excellent agreement of the MEPs

Table 3. Comparison of the Locations of the Shepard Points in QM-MCMM and in QM/MM-MCMM Dynamics Calculations for the Reaction OH + Propane (R1)[a]

	QM-MCMM		QM/MM-MCMM	
*n*th point	s	E	s	E
0[b]	0.00	4.91	0.00	4.72
1	−0.51	4.26	−0.52	4.07
2	0.19	4.09	0.19	3.93
3	−1.22	3.08	−1.21	2.95
4	0.29	2.48	0.29	2.36
5	−2.11	1.85	−2.08	1.77
6	−0.45	4.29	−0.45	4.13
7	0.53	−3.49	0.53	−3.72
8H	−2.54	N/a	−2.51	N/a
8L	0.51	N/a	0.51	N/a
8	N/a	7.75	N/a	7.54
9H	−2.79	N/a	−2.77	N/a
9L	0.96	N/a	0.97	N/a
9	N/a	6.15	N/a	6.07
10H	−2.79	N/a	−2.77	N/a
10L	0.96	N/a	0.97	N/a
10	N/a	2.56	N/a	2.17

[a] Only Shepard points for which QM or QM/MM calculations are needed are listed, thus excluding the reactant well and the product well. Energy in kcal/mol, and s in bohr. The scheme that was presented in ref 14 and summarized in Table S1 in ref 16 is adopted for determination of the locations of the Shepard points. See the cited references for details. The *n*th Shepard point is determined on the basis of the MCMM-(*n* − 1) potential energy surface, and, therefore, the s value listed for the *n*th point is corresponding to the MEP in the MCMM-(*n* − 1) potential energy surface. Reaction take place at the C1 position. The MPW1K/DIDZ level of theory in QM calculations and MM3 force field for MM calculations. See Figure 1 for the QM/MM boundary setup. The mechanical embedding scheme was used in QM/MM computations. [b] The saddle point.

calculated by the QM/MM-MCMM and QM-MCMM schemes, as illustrated in Figure 3(A). For reaction R2, the difference between the QM/MM and QM barrier heights is larger (about 1 kcal/mol) than that for reaction R1.

The QM geometries for the saddle points are also reproduced well by the QM/MM computations. The bond distances for the breaking/forming bonds generally agree within 0.02 Å between the QM and QM/MM results. The only exception is for reaction R2, where the distance between the O atom in the OH radical and the H atom being transferred has been shortened by 0.04 Å for the *exo* H5a atom in QM/MM computations.

Turning to the vibrational frequencies, one finds in Table 2 that there are usually several tens of wavenumbers deviations on average between the QM/MM and QM calculations, as indicated by the mean unsigned deviation (MUD). However, it is the mean signed deviation (MSD) that is more important in determination of the zero point energy, because the difference in the errors of the transition state and reactant zero point energies has a large effect on dynamics calculations if vibrational frequencies are not scaled in the dynamics step. The MSD is −32 cm^{-1} for the reactant, −26 cm^{-1} for the saddle point, and −35 cm^{-1} for the product in reaction R1. For reaction R2, the MSDs are close to −60 cm^{-1}, with a variation as small as 1 cm^{-1}. As noted previously in section II.C, the same trend of over- or

Multiconfiguration Molecular Mechanics

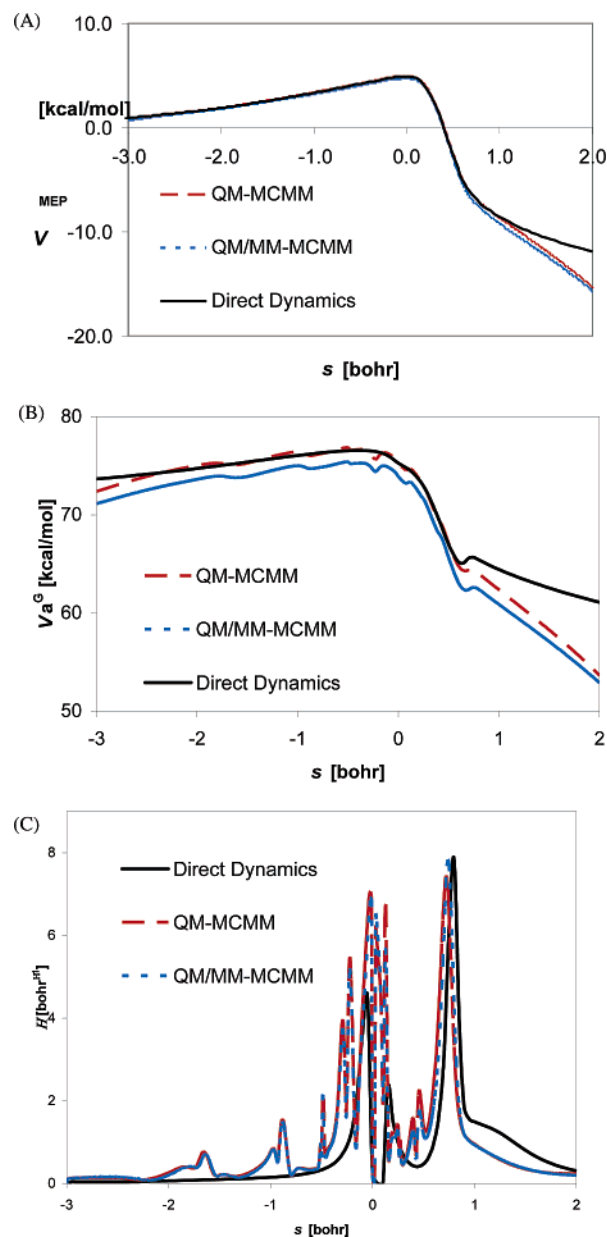*J. Chem. Theory Comput., Vol. 2, No. 5, 2006* **1247**

Figure 3. (A) The classical potential energy curve, V_{MEP}, (B) the vibrational adiabatic ground-state potential energy curve, V_a^G, and (C) the reaction-path curvature reaction, κ, as functions of reaction coordinate s for the reaction OH with propane (R1).

Table 4. Convergence of TST, CVT, CVT/SCT, and CVT/μOMT with Respect to the Number of Nonstationary Hessians for QM/MM-MCMM-X (X = 2, 4, 6, 8, 10) at T = 300 and 600 K for the R1 Reaction OH + Propane[a]

T (K)	TST	CVT	CVT/SCT	CVT/μOMT
		MCMM-0		
300	0.0	108.8	1346.3	1334.4
600	0.0	40.0	153.2	151.2
		MCMM-2		
300	0.0	−34.3	36.8	35.7
600	0.0	−25.0	−0.8	−1.6
		MCMM-4		
300	0.0	−33.3	−26.4	−27.0
600	0.0	−24.2	−12.1	−12.8
		MCMM-6		
300	0.0	0.7	0.8	0.0
600	0.0	2.4	2.4	1.6
		MCMM-8		
300	0.0	0.0	0.0	−0.8
600	0.0	0.8	0.8	0.0
		MCMM-10		
300	0.0	0.0	0.0	0.0
600	0.0	0.0	0.0	0.0

[a] Convergence is indicated by $(k_{QM/MM-MCMM-X} - k_{QM/MM-MCMM-10})/k_{QM/MM-MCMM-10} \times 100$.

Table 5. Convergence of TST, CVT, CVT/SCT, and CVT/μOMT with Respect to the Number of Nonstationary Hessians for QM/MM-MCMM-X (X = 2, 4, 6, 8, 10) at T = 300 and 600 K for the R2 Reaction OH + Camphor[a]

T (K)	TST	CVT	CVT/SCT	CVT/μOMT
		MCMM-0		
300	0.0	26.5	26.8	26.8
600	0.0	−8.8	−9.8	−9.8
		MCMM-2		
300	0.0	3.2	−19.5	−19.5
600	0.0	2.9	−3.3	−3.3
		MCMM-4		
300	0.0	4.5	11.0	11.0
600	0.0	3.6	5.9	5.9
		MCMM-6		
300	0.0	0.0	−1.3	−1.3
600	0.0	0.0	0.0	0.0
		MCMM-8		
300	0.0	0.0	1.1	1.4
600	0.0	0.0	0.7	0.7
		MCMM-10		
300	0.0	0.0	0.0	0.0
600	0.0	0.0	0.0	0.0

[a] Convergence is indicated by $(k_{QM/MM-MCMM-X} - k_{QM/MM-MCMM-10})/k_{QM/MM-MCMM-10} \times 100$.

underestimation of a vibrational frequency along the reaction path leads to significant cancellation of error in evaluating the relative free energy profile and vibrational partition functions. This rationalizes why QM/MM-MCMM gives reasonable rate constants compared with QM-MCMM. As a result, the vibrationally adiabatic ground-state potential energy curve, V_a^G, looks very similar in the QM/MM-MCMM and the QM-MCMM dynamics calculations, as demonstrated in Figure 3(B) for reaction R1.

The coupling between the motion along the reaction coordinate and the spectator coordinates is very similar in the QM/MM-MCMM and QM-MCMM dynamics calculations. Taking reaction R1 as an example, the reaction-path curvature, which is an indication of such coupling, shows very small differences between QM/MM-MCMM and QM-

MCMM dynamics calculations, as depicted in Figure 3(C). The underlying mechanism is that usually the coupling is significant only for those atoms that are close to the atoms directly involved in bond breaking and bond forming, and often those atoms are included in the PS, which is treated at the QM level. Thus, QM/MM-MCMM dynamics essentially

Table 6. Rate Constants Calculated by the Direct Dynamics, by the QM-MCMM Dynamics, and by the QM/MM-MCMM Dynamics for the Reaction OH + Propane (Reaction R1)[a]

T (K)	TST	CVT	CVT/SCT	CVT/LCT(0)	CVT/LCT	CVT/μOMT
			Direct Dynamics			
200	6.55E−16	2.89E−17	5.59E−17	4.64E−17	4.77E−17	5.59E−17
300	1.12E−14	1.46E−15	1.92E−15	1.77E−15	1.80E−15	1.92E−15
400	5.43E−14	1.19E−14	1.37E−14	1.31E−14	1.32E−14	1.37E−14
500	1.58E−13	4.60E−14	4.97E−14	4.84E−14	4.86E−14	4.97E−14
600	3.53E−13	1.22E−13	1.28E−13	1.25E−13	1.26E−13	1.28E−13
1000	2.73E−12	1.23E−12	1.24E−12	1.23E−12	1.23E−12	1.24E−12
			QM-MCMM			
200	6.55E−16	1.54E−17	5.25E−17	4.12E−17	4.35E−17	5.34E−17
300	1.12E−14	9.82E−16	1.74E−15	1.56E−15	1.61E−15	1.76E−15
400	5.43E−14	8.99E−15	1.25E−14	1.17E−14	1.20E−14	1.26E−14
500	1.58E−13	3.74E−14	4.64E−14	4.45E−14	4.51E−14	4.67E−14
600	3.53E−13	1.04E−13	1.21E−13	1.18E−13	1.19E−13	1.22E−13
1000	2.73E−12	1.11E−12	1.04E−12	1.02E−12	1.03E−12	1.04E−12
			QM/MM-MCMM			
200	9.71E−15	2.82E−17	8.15E−17	6.49E−17	6.78E−17	8.26E−17
300	1.46E−13	1.48E−15	2.42E−15	2.18E−15	2.23E−15	2.44E−15
400	6.60E−13	1.24E−14	1.63E−14	1.54E−14	1.57E−14	1.64E−14
500	1.84E−12	4.82E−14	4.94E−14	4.76E−14	4.80E−14	4.96E−14
600	3.99E−12	1.25E−13	1.24E−13	1.21E−13	1.22E−13	1.25E−13
1000	2.90E−11	1.22E−12	1.17E−12	1.16E−12	1.16E−12	1.17E−12

[a] Reaction takes place at the C1 position. The MPW1K/DIDZ level of theory in QM calculations and MM3 force field for MM calculations. See Figure 1 for the QM/MM boundary setup. The mechanical embedding (ME) scheme was used in QM/MM computations. The MCMM-10 results are listed for MCMM dynamics calculations. The rate constant including tunneling is then given by $k^{CVT/MT} = \kappa^{MT} k^{CVT}$, where κ^{MT} is the transmission coefficient, and MT is SCT, LCT(0), LCT, or μOMT. The definitions of these abbreviations are given in footnote *a* of Table 8.

Table 7. Rate Constants Calculated by the QM-MCMM Dynamics and by the QM/MM-MCMM Dynamics for the Reaction OH + Camphor (Reaction R2)[a,b]

T (K)	TST	CVT	CVT/SCT	CVT/LCG0	CVT/LCG	CVT/μOMT
			QM-MCMM			
200	1.29E−13	3.92E−15	9.28E−15	8.26E−15	8.64E−15	9.30E−15
300	2.22E−13	2.52E−14	3.81E−14	3.59E−14	3.68E−14	3.81E−14
400	3.39E−13	7.42E−14	9.41E−14	9.08E−14	9.22E−14	9.42E−14
500	4.89E−13	1.57E−13	1.83E−13	1.79E−13	1.81E−13	1.83E−13
600	6.82E−13	2.78E−13	3.10E−13	3.05E−13	3.07E−13	3.10E−13
1000	2.01E−12	1.08E−12	7.65E−13	7.60E−13	7.62E−13	7.65E−13
			QM/MM-MCMM			
200	3.53E−14	1.95E−16	5.38E−16	4.35E−16	1.14E−15	1.16E−15
300	1.17E−13	4.00E−15	6.30E−15	5.71E−15	1.01E−14	1.02E−14
400	2.52E−13	2.08E−14	2.69E−14	2.54E−14	3.66E−14	3.67E−14
500	4.51E−13	6.19E−14	7.27E−14	7.01E−14	9.00E−14	9.03E−14
600	7.27E−13	1.37E−13	1.53E−13	1.50E−13	1.79E−13	1.79E−13
1000	2.93E−12	9.47E−13	9.85E−13	9.76E−13	1.05E−12	1.05E−12

[a] The MPWB1K/DIDZ level of theory in QM calculations and CHARMM27 force field for MM calculations. See Table S1 in the Supporting Information for augmented MM parameters. See Figure 2 for the QM/MM boundary setup. The electrostatic embedding (EE) scheme redistributed charge and dipole (RCD) was used in QM/MM computations. The MCMM-10 results are listed. The rate constant including tunneling is then given by $k^{CVT/MT} = \kappa^{MT} k^{CVT}$, where κ^{MT} is the transmission coefficient, and MT is SCT, LCT(0), LCT, or μOMT, which are defined in footnote *a* of Table 8. [b] Abstraction of *exo* H5a.

retains the feature of reaction-path curvature of the QM-MCMM dynamics. This also implies that, under certain circumstances, one could use effective reduced-dimensional resonance matrix element, V_{12}^{eff}, to replace the full-dimensional resonance matrix element, V_{12}, in the MCMM expression eq 2, without losing much accuracy in MCMM dynamics calculations.

Tables 4 and 5 are the main results of the present paper. They show that the rate constants converge well with respect to the number of Hessians at nonstationary points. In particular, all MCMM-6 and MCMM-8 calculations in the two tables agree with the MCMM-10 calculations within 2%. The noticeably better convergence for reaction R2 as compared to R1 comes primarily from a more realistic description of the van der Waals energy for R2 in the repulsion region (see section IV.B). In another article, we will show that by using appropriate MM functions, more accurate MCMM surfaces can be generated with a fewer number of Hessians.[82]

If QM/MM provides good agreement with QM for barrier heights, vibrations, energies of reaction, and barrier heights,

Multiconfiguration Molecular Mechanics

J. Chem. Theory Comput., Vol. 2, No. 5, 2006 **1249**

Table 8. Percentage Deviations of Reaction Rates in QM-MCMM and QM/MM-MCMM Dynamics (with Respect to Direct Dynamics) for the Reaction of OH + Propane (R1)[a]

T (K)	TST	CVT	CVT/ SCT	CVT/ LCT(0)	CVT/ LCT	CVT/ μOMT
			QM-MCMM			
200	0	−47	−6	−11	−9	−4
300	0	−33	−9	−12	−11	−8
400	0	−24	−9	−11	−9	−8
500	0	−19	−7	−8	−7	−6
600	0	−15	−5	−6	−6	−5
1000	0	−10	−16	−17	−16	−16
MSPE[b]	0	−25	−9	−11	−10	−8
MUPE[c]	0	25	9	11	10	8
			QM/MM-MCMM			
200	1382	−2	46	40	42	48
300	1204	1	26	23	24	27
400	1115	4	19	18	19	20
500	1065	5	−1	−2	−1	0
600	1030	2	−3	−3	−3	−2
1000	962	−1	−6	−6	−6	−6
MSPE[b]	1126	2	14	12	12	14
MUPE[b]	1126	3	17	15	16	17

[a] Reaction takes place at the C1 position. The MPW1K/DIDZ level of theory in QM calculations and MM3 force field for MM calculations. See Figure 1 for the QM/MM boundary setup. The mechanical embedding scheme was used in QM/MM computations. The MCMM-10 results are listed for MCMM dynamics calculations. The rate constant including tunneling is then given by $k^{CVT/MT} = \kappa^{MT} k^{CVT}$, where κ^{MT} is the transmission coefficient, and MT is SCT, LCT(0), LCT, or μOMT. The transmission coefficients are defined as follows: SCT, small-curvature tunneling; LCT(0), large-curvature tunneling only considering unexcited diabatic tunneling states; LCT, full large-curvature tunneling; μOMT, microcanonically optimized multidimensional tunneling. [b] MeanSigned Percentage Deviation (MSPD) averaged over six temperatures. [c] MeanUnsigned Percentage Deviation (MUPD) averaged over six temperatures.

QM/MM-MCMM dynamics should yield rate constants comparable with QM-MCMM dynamics calculations. The R1 reaction in the present study is a nice example that confirms this expectation: the QM and QM/MM barrier heights differ slightly (by 0.2 kcal/mol), and the QM and QM/MM rate constants agree with each other generally within 25%, as can be seen from Tables 4 and 6. Here, we should point out that it is more meaningful to compare the rate constants with tunneling contributions, e.g., CVT/SCT rate constants, than the rate constants determined by just one point at the reaction path, e.g., the CVT rate constants, because the nontunneling calculations are more vulnerable to the numerical noise in the computations; the calculation of the tunneling contributions involves integration over the reaction path, and this reduces the numerical noises significantly (since performing an integral is like performing an average). The barrier heights for the pathway of reaction R2 that we studied show larger discrepancies (about 1 kcal/mol) in QM and QM/MM computations, in comparison with the R1 case. The bigger errors in the R2 barrier height are not surprising, since the QM/MM boundary in R2 is closer to the C atom that is directly involved in bond-breaking, and one therefore expects more pronounced boundary effects due to the mismatch between the QM and MM energy ap-

Table 9. Percentage Deviations of Reaction Rates in QM/MM-MCMM Dynamics (with Respect to QM-MCMM Dynamics) for the Reaction of OH + Camphor (Reaction R2)[a,b]

T (K)	TST	CVT	CVT/ SCT	CVT/ LCT(0)	CVT/ LCT	CVT/ μOMT
200	−73	−95	−94	−95	−87	−88
300	−47	−84	−83	−84	−73	−73
400	−26	−72	−71	−72	−60	−61
500	−8	−61	−60	−61	−50	−51
600	7	−51	−51	−51	−42	−42
1000	46	−12	29	28	38	37
MSPE[c]	−17	−62	−55	−56	−46	−46
MUPE[d]	34	62	65	65	58	59

[a] The MPWB1K/DIDZ level of theory in QM calculations and CHARMM27 force field for MM calculations. See Table S1 in the Supporting Information for augmented MM parameters. See Figure 2 for the QM/MM boundary setup. The electrostatic embedding (EE) scheme redistributed charge and dipole (RCD) was used in QM/MM computations. The MCMM-10 results are listed. The rate constant including tunneling is then given by $k^{CVT/MT} = \kappa^{MT} k^{CVT}$, where κ^{MT} is the transmission coefficient, and MT is SCT, LCT(0), LCT, or μOMT. The definitions of the transmission coefficients are given in footnote *a* of Table 8. [b] Abstraction of the *exo* H5a. [c] MeanSigned Percentage Deviation (MSPD) averaged over six temperatures. [d] MeanUnsigned Percentage Deviation (MUPD) averaged over six temperatures.

proximations. Generally speaking, a 1 kcal/mol difference from QM calculations is quite reasonable for QM/MM calculations. Unfortunately, though, a difference as small as 1 kcal/mol in energy can produce a large difference in rates, the effect being more pronounced at low temperatures, as demonstrated in Tables 5 and 7. Reactions R1 and R2 serve as examples at two extremes to illustrate how the accuracy of QM/MM energetic information affects the accuracy of QM/MM-MCMM dynamics.

VII. Concluding Remarks

In this paper, we introduced a new MCMM algorithm, which is called QM/MM-MCMM, for studies of very large reactive systems. The QM/MM-MCMM method uses QM/MM calculations to generate the resonance matrix element V_{12} of MCMM calculations, and it is tested for two hydrogen-transfer reactions by comparing QM/MM-MCMM calculations to MCMM calculations in which the resonance matrix element is generated by full QM calculations, which is called QM-MCMM, and also, for one reaction, by comparing to full QM direct dynamics calculations where the potential energies are computed quantum mechanically on the fly. Very encouraging results are obtained for rate constants including tunneling contributions, when the QM/MMM method adequately reproduces the barrier height of the QM calculations, thereby validating the QM/MM-MCMM method as a very general and efficient procedure for generating potential energy surfaces for large reactive systems. As full QM calculations are usually not possible for very large systems such as proteins or large nanoparticle catalysts, QM/MM-MCMM is an alternative practical way to QM-MCM in study of these reactive systems. However, as illustrated by the cautionary example of reaction R2, one will not get as reliable results if the QM/MM calculations introduce an error in the barrier height.

The resonance matrix element V_{12} plays the central role in the MCMM method and in other methods based on valence bond theory. An advantage of our MCMM algorithm, as discussed in the Introduction, is that the full dimensionality of the resonance matrix element V_{12} is included. Does one really need a full-dimensional resonance integral in all cases? For a large system, a full-dimensional resonance integral might cause technical problems in handling (computing and storing) very large Hessian matrices. Could one replace V_{12} by a reduced-dimensional effective resonance integral in the MCMM expression eq 2 without losing much accuracy in the MCMM dynamics calculations? If yes, how can we construct the effective reduced-dimensional resonance integral?

It seems that, in many cases, significant coupling between the motion along the reaction coordinate and other motions is present only for atoms that are within a small distance from the active center. That is, dynamical coupling seems rather localized near to the bond-breaking and bond-forming atoms. This justifies the use of a reduced-dimensional resonance integral, provided that the dynamical coupling is adequately described. Please note that even though the reduced-dimensional resonance integral is used, the MCMM potential is still full dimensional. In other words, one approximates the full-dimensional MCMM potential based on the full-dimensional resonance integral by a full-dimensional MCMM based on a reduced-dimensional resonance integral.

Now we consider the second question: how to construct the effective reduced-dimensional resonance integral? The most simplified possible reduced-dimensional effective resonance integral is a constant. Although for some reactions, the resonance matrix element is almost constant along the MEP, we found that it must sometimes vary appreciably off the MEP in order to give reasonable frequencies.[13] Therefore, the assumption that the resonance matrix element is constant in the reaction swath is probably oversimplified for many cases.

By fitting the resonance integral to a simple analytic function, like an exponential function or Gaussian, one increases the flexibility of a reduced-dimensionality scheme, and by selecting the parameters carefully, one might be able to reproduce some desired properties such as the experimental barrier height or theoretically calculated vibrational frequencies at the saddle point. The problem of this kind of treatment is that it is difficult to find an analytical function that is generally applicable for different reactions and systematically improvable by including more and more kinetic and electronic-structure information.

In comparison with simple analytic functions, Shepard interpolation is a general and systematically improvable algorithm for constructing the resonance surface. Therefore a way to construct a reduced-dimensional effective resonance integral is by Shepard interpolation based on QM or QM/MM calculations in which the resonance integral explicitly depends on only a subset of the atoms, e.g., the atoms in the model system (the atoms in the active center and possibly some nearby spectator atoms). We will focus our discussion on this point in the remaining text.

The most direct treatment for reducing the dimensionality of the resonance integral is to perform cluster QM calculations for a model system. As an example, we note that Sierka and Sauer[123] explored a idea of combining a method they call QM-Pot with the empirical valence-bond theory in studying proton-transfer reactions in zeolite catalysts; QM-Pot,[101] which stands for the "combined quantum mechanics-interatomic potential functions approach", is a mechanical-embedding QM/MM algorithm in the language we use, but they prefer to reserve "molecular mechanics" for traditional organic and biological force fields. In ref 123, the authors started by doing QM calculations on a model system, then parametrized these with an EVB potential function, and proceeded to generate an initial guess (geometry and Hessian) for minima and saddle points for the entire system based on the parametrized EVB potential for the model system and the interatomic potential between the model system and its surroundings; finally they optimized those stationary points (the minima and the saddle point) employing the QM-Pot approach. Their way of combining the EVB for a model system and the interatomic potentials between the model system and its environment can be regarded as Cluster-QM-MCMM, or CQM-MCMM, because the resonance matrix element V_{12} is derived from a cluster model for the active site, which differs from our QM/MM-MCMM treatment where V_{12} is derived from QM/MM calculations for the entire system.

Cluster QM calculations are much less expensive, and they can produce good results in many cases if used with care. However, a key problem of the cluster QM calculations is whether the model system is a faithful model for the active center of the entire system as the electronic structure changes during the reaction. Although the dynamical coupling seems rather localized near to the bond-breaking and bond-forming atoms, the environment (e.g., the solvent) may perturb the electronic structure of the atoms in the active center by imposing geometric constraints and/or by polarization. Such effects can be critical in some cases, e.g. when the model system contains transition metals and has more than one energetically low-lying electronic state.[172] A model system in the gas phase might not be a wise choice in such a situation, and QM/MM calculations, in particular electrostatic-embedding QM/MM calculations, are recommended, if full QM calculations for the entire system are not feasible. If a model system does not provide a good representation of the electronic structure of the reaction center, we doubt that one can get a correct potential surface for the entire system by improving only the diagonal terms V_{11} and V_{22}, with the resonance integral based on that inappropriate model system. In particular, we question whether it is appropriate to use a resonance integral calculated in the gas phase for condensed-phase systems. A detailed and systematic examination of this issue would be worthwhile.

Then how should one get the effective reduced-dimensional resonance integral from full-dimensional QM or QM/MM calculations? One possible way is to treat explicitly the degrees of freedom of the atoms in the model system while considering the environment as a bath. One might optimize the geometry of the environment for a given geometry of

the active center, i.e., force the environment to follow the reaction in the active site adiabatically, and evaluate the resonance integral accordingly. A more elaborate scheme would be to perform an ensemble average and use the averaged resonance integral as the effective resonance integral. After doing that, one simply retains in the resonance integral the degrees of freedom of the atoms in the active site. These schemes are surely more complicated than the scheme based on cluster QM calculations, but they have the reward that the resonance integral is obtained, instead of by a gas-phase model, by a more realistic model that it is probably more accurate.

In the Introduction we compared the present QM/MM-MCMM approach to another possible approach, called MCMM/MM. Whereas the former corresponds to putting QM/MM into MCMM, the latter corresponds to putting MCMM into QM/MM. We pointed out that MCMM/MM would not contain the effects of the SS in the quantum mechanical description of the PS, that is, it would correspond to mechanical embedding, whereas the present approach allows one to use, as is done in the present applications, either a mechanical embedding QM/MM method or an electrostatic embedding QM/MM method, which provides a more realistic description. (We demonstrated both mechanical and electrostatic embedding schemes in this study.) In addition to this question of the interaction of the subsystems, there are also computational considerations involved in the strategy we have chosen, as we discuss next.

First, MCMM/MM requires QM calculations on an isolated model system (as in the cluster-QM/MCMM that we discussed above), which are much simpler than doing QM/MM computation for the entire system. For example, finding the QM/MM transition-state structure for the entire system is in general much harder than finding the QM transition-state structure for the isolated model system.

Second, we note that MCMM/MM does not need to handle large Hessian matrices when constructing V_{12}, while in QM/MM-MCMM, unless one uses a reduced-dimensional representation for V_{12}, it is necessary to manipulate a full-dimensional Hessian matrix, whose size increases as N^2 (N is the number of the atoms). Not only is such a big Hessian matrix expensive in calculations but also it presents a problem in storage. Moreover, most electronic-structure programs provide analytic derivatives for the PS atoms but not for the SS atoms, which are treated as background point charges in an electrostatic embedding QM/MM computation. Thus, MCMM/MM is less computationally demanding for large-size systems.

Finally, we add a note on MCMM parametrization. It is always a great advantage if the effort required for parametrization is limited. When using MCMM/MM we actually implicitly assume that the MCMM potential is transferable between different conformations of the entire system. (This may be also true for QM/MM-MCMM employing a reduced-dimensional effective V_{12}.) A greater degree of transferability could be achieved by regarding the PS as a reacting functional group, which is present in various parts of a system or in different systems, just like a residue in proteins interacting with the solvent water molecules. Thus, one might

develop a set of MCMM potentials for selected reactions and use them as reactive MM potentials for standard MD simulations, e.g., to simulate the hydrogen exchange between water molecules and a solvated protein, the exchange taking place for various residues at the same time. Here, one would assume that the reactions are taking place at the same time at different locations without interference between each other, which is equivalent to approximating a large (valence-bond theory) matrix by several sub-blocks neglecting the off-diagonal elements among the sub-blocks. This kind of transferability would permit MCMM/MM and/or QM/MM-MCMM with a reduced-dimensional V_{12} to be treated as generalized MM potentials for simulating reactive biomolecules.

Supporting Information Available: Detailed description of the MM parameters used for reaction R2, the optimized geometries for the reactant and products for reaction R2 at the QM, MM, and QM/MM levels of theory, the redundant internal coordinates used for generalized normal-mode analyses for reaction R2, and the vibrational frequencies that are computed at the QM and QM/MM levels for reactions R1 and R2. This material is available free of charge via the Internet at http://pubs.acs.org.

References

(1) Wang, I. S. Y.; Karplus, M. *J. Am. Chem. Soc.* **1973**, *95*, 8160.

(2) Warshel, A.; Karplus, M. *Chem. Phys. Lett.* **1975**, *32*, 11.

(3) Leforestier, C. *J. Chem. Phys.* **1978**, *68*, 4406.

(4) Truhlar, D. G.; Duff, J. W.; Blais, N. C.; Tully, J. C.; Garrett, B. C. *J. Chem. Phys.* **1982**, *72*, 764.

(5) Car, R.; Parrinello, M. *Phys. Rev. Lett.* **1985**, *55*, 2471.

(6) Baldridge, K. K.; Gordon, M. S.; Steckler, R.; Truhlar, D. G. *J. Phys. Chem.* **1989**, *93*, 5107.

(7) Truhlar, D. G.; Gordon, M. S. *Science* **1990**, *249*, 491.

(8) Garrett, B. C.; Melius, C. F.; Page, M. In *Theoretical and Computational Models for Organic Chemistry*; Formosinho, S. J., Csizmadia, I. G., Arnaut, L. G., Eds.; Kluwer: Dordrecht, 1991; p 35.

(9) Uggerud, E.; Helgaker, T. *J. Am. Chem. Soc.* **1992**, *114*, 4265.

(10) Woo, T. K.; Margl, P. M.; Ziegler, T.; Blöchl, P. E. *J. Phys. Chem. B* **1997**, *101*, 7877.

(11) Bolton, K.; Hase, W. L.; Peslherbe, G. H. In *Modern Methods for Multidimensional Dynamics Calculations in Chemistry*; Thompson, D. C., Ed.; World Scientific: Singapore, 1998; p 143.

(12) Li, X.; Millam, J. M.; Schlegel, H. B. *J. Chem. Phys.* **2000**, *113*, 10062.

(13) Kim, Y.; Corchado, J. C.; Villa, J.; Xing, J.; Truhlar, D. G. *J. Chem. Phys.* **2000**, *112*, 2718.

(14) Albu, T. V.; Corchado, J. C.; Truhlar, D. G. *J. Phys. Chem. A* **2001**, *105*, 8465.

(15) Truhlar, D. G. *J. Phys. Chem. A* **2002**, *106*, 5048.

(16) Lin, H.; Pu, J. Z.; Albu, T. V.; Truhlar, D. G. *J. Phys. Chem. A* **2004**, *108*, 4112.

(17) Kim, K. H.; Kim, Y. *J. Chem. Phys.* **2004**, *120*, 623. Kim, Y.; Kim, Y. *J. Phys. Chem. A* **2006**, *110*, 60.

(18) Olson, W. K.; Flory, P. J. *Biopolymers* **1972**, *11*, 25.

(19) van Gunsteren, W. F.; Berendsen, H. J. C.; Geurtsen, R. G.; Zwinderman, H. R. J. *Ann. N. Y. Acad. Sci.* **1986**, *482*, 287.

(20) Allinger, N. L.; Yuh, Y. H.; Lii, J. H. *J. Am. Chem. Soc.* **1989**, *111*, 8551.

(21) Lii, J. H.; Allinger, N. L. *J. Am. Chem. Soc.* **1989**, *111*, 8566.

(22) Lii, J. H.; Allinger, N. L. *J. Am. Chem. Soc.* **1989**, *111*, 8576.

(23) Mayo, S. L.; Olafson, B. D.; Goddard, W. A., III. *J. Phys. Chem.* **1990**, *94*, 8897.

(24) Rappé, A. K.; Casewit, C. J.; Colwell, K. S.; Goddard, W. A., III; Skid, W. M. *J. Am. Chem. Soc.* **1992**, *114*, 10024.

(25) Casewit, C. J.; Colwell, K. S.; Rappé, A. K. *J. Am. Chem. Soc.* **1992**, *114*, 10035. Casewit, C. J.; Colwell, K. S.; Rappé, A. K. *J. Am. Chem. Soc.* **1992**, *114*, 10046.

(26) Pearlman, D. A.; Case, D. A.; Caldwell, J. W.; Ross, W. S.; Cheatham, T. E. I.; DeBolt, S.; Ferguson, D.; Seibel, G.; Kollman, P. A. *Comput. Phys. Commun.* **1995**, *91*, 1.

(27) Rappé, A. K.; Colwell, K. S.; Casewit, C. J. *Inorg. Chem.* **1993**, *32*, 3438.

(28) Cornell, W. D.; Cieplak, P.; Bayly, C. I.; Gould, I. R.; Merz, K. M., Jr.; Ferguson, D. M.; Spellmeyer, D. C.; Fox, T.; Caldwell, J. W.; Kollman, P. A. *J. Am. Chem. Soc.* **1995**, *117*, 5179.

(29) Hill, J.-R.; Sauer, J. *J. Phys. Chem.* **1994**, *98*, 1238. Hill, J.-R.; Sauer, J. *J. Phys. Chem.* **1995**, *99*, 9536.

(30) Jorgensen, W. L.; Maxwell, D. S.; Tirado-Rives, J. *J. Am. Chem. Soc.* **1996**, *118*, 11225.

(31) Halgren, T. A. *J. Comput. Chem.* **1996**, *17*, 490. Halgren, T. A. *J. Comput. Chem.* **1996**, *17*, 520. Halgren, T. A. *J. Comput. Chem.* **1996**, *17*, 552.

(32) Halgren, T. A.; Nachbar, R. B. *J. Comput. Chem.* **1996**, *17*, 587.

(33) Halgren, T. A. *J. Comput. Chem.* **1996**, *17*, 616.

(34) Sierka, M.; Sauer, J. *Faraday Discuss.* **1997**, *106*, 41.

(35) Schröder, K.-P.; Sauer, J. *J. Phys. Chem.* **1996**, *100*, 11043.

(36) Landis, C. R.; Cleveland, T.; Firman, T. K. *J. Am. Chem. Soc.* **1998**, *120*, 2641.

(37) MacKerell, A. D., Jr.; Bashford, D.; Bellott, M.; Dunbrack, R. L.; Evanseck, J. D.; Field, M. J.; Fischer, S.; Gao, J.; Guo, H.; Ha, S.; Joseph-McCarthy, D.; Kuchnir, L.; Kuczera, K.; Lau, F. T. K.; Mattos, C.; Michnick, S.; Ngo, T.; Nguyen, D. T.; Prodhom, B.; Reiher, W. E., III.; Roux, B.; Schlenkrich, M.; Smith, J. C.; Stote, R.; Straub, J.; Watanabe, M.; Wiorkiewicz-Kuczera, J.; Yin, D.; Karplus, M. *J. Phys. Chem. B* **1998**, *102*, 3586.

(38) McDonald, N. A.; Jorgensen, W. L. *J. Phys. Chem. B* **1998**, *102*, 8049.

(39) Jorgensen, W. L.; McDonald, N. A. *THEOCHEM* **1998**, *424*, 145.

(40) Rizzo, R. C.; Jorgensen, W. L. *J. Am. Chem. Soc.* **1999**, *121*, 4827.

(41) Ewig, C. S.; Thacher, T. S.; Hagler, A. T. *J. Phys. Chem. B* **1999**, *103*, 6999.

(42) Allinger, N. L.; Durkin, K. A. *J. Comput. Chem.* **2000**, *21*, 1229.

(43) Firman, T. K.; Landis, C. R. *J. Am. Chem. Soc.* **2001**, *123*, 11728.

(44) Kaminski, G. A.; Friesner, R. A.; Tirado-Rives, J.; Jorgensen, W. L. *J. Phys. Chem. B* **2001**, *105*, 6474.

(45) Price, M. L. P.; Ostrovsky, D.; Jorgensen, W. L. *J. Comput. Chem.* **2001**, *22*, 1340.

(46) Ren, P.; Ponder, J. W. *J. Comput. Chem.* **2002**, *23*, 1497.

(47) Ponder, J. W.; Case, D. A. *Adv. Protein Chem.* **2003**, *66*, 27.

(48) London, F. *Z. Elektrochem.* **1929**, *35*, 552.

(49) Eyring, H.; Polanyi, M. *Z. Phys. Chem. B* **1931**, *12*, 279.

(50) Kimball, G. E.; Eyring, H. *J. Am. Chem. Soc.* **1932**, *54*, 3876.

(51) Coulson, C. A.; Danielsson, U. *Arkiv Fysik* **1954**, *8*, 245.

(52) Sato, S. *J. Chem. Phys.* **1955**, *23*, 2465.

(53) Porter, R. N.; Karplus, M. *J. Chem. Phys.* **1964**, *40*, 1105.

(54) Parr, C. A.; Truhlar, D. G. *J. Phys. Chem.* **1971**, *75*, 1844.

(55) Raff, L. M. *J. Chem. Phys.* **1974**, *60*, 2220.

(56) Warshel, A.; Weiss, R. M. *J. Am. Chem. Soc.* **1980**, *102*, 6218.

(57) Chang, Y.-T.; Minichino, C.; Miller, W. H. *J. Chem. Phys.* **1992**, *96*, 4341.

(58) Minichino, C.; Voth, G. A. *J. Phys. Chem. B* **1997**, *101*, 4544.

(59) Okuyama-Yoshida, N.; Nagaoka, M.; Yamabe, T. *J. Phys. Chem. A* **1998**, *102*, 285.

(60) Lefohn, A. E.; Ovchinnikov, M.; Voth, G. A. *J. Phys. Chem. B* **2001**, *105*, 6628.

(61) Åqvist, J.; Warshel, A. *Chem. Rev.* **1993**, *93*, 2523.

(62) Schlegel, H. B.; Sonnenberg, J. L. *J. Chem. Theory Comput.* **2006**, *2*, 905.

(63) Whitlock, P. A.; Muckerman, J. T.; Fisher, E. R. *J. Chem. Phys.* **1982**, *76*, 4468.

(64) Bernardi, F.; Olivucci, M.; Robb, M. A. *J. Am. Chem. Soc.* **1992**, *114*, 1606.

(65) Halvick, P.; Truhlar, D. G. *J. Chem. Phys.* **1992**, *96*, 2895.

(66) Caltaneo, P.; Persico, M. *Theor. Chem. Acc.* **2000**, *103*, 390.

(67) Ischtwan, J.; Collins, M. A. *J. Chem. Phys.* **1994**, *100*, 8080.

(68) Nguyen, K. A.; Rossi, I.; Truhlar, D. G. *J. Chem. Phys.* **1995**, *103*, 5522.

(69) Truhlar, D. G.; Brown, F. B.; Steckler, R.; Isaacson, A. D. In *The Theory of Chemical Reaction Dynamics*; Clary, D. C., Ed.; NATO ASI Series C, Reidel: Dordrecht, 1986; Vol. 170, p 285.

(70) Marcus, R. A.; Coltrin, M. E. *J. Chem. Phys.* **1977**, *67*, 2609.

(71) Skodje, R. T.; Truhlar, D. G.; Garrett, B. C. *J. Phys. Chem.* **1981**, *85*, 3019.

(72) Skodje, R. T.; Truhlar, D. G.; Garrett, B. C. *J. Chem. Phys.* **1982**, *78*, 1213.

(73) Liu, Y. P.; Lynch, G. C.; Truong, T. N.; Lu, D. H.; Truhlar, D. G.; Garrett, B. C. *J. Am. Chem. Soc.* **1993**, *115*, 2408.

Multiconfiguration Molecular Mechanics

J. Chem. Theory Comput., Vol. 2, No. 5, 2006 **1253**

(74) Lu, D.-h.; Truong, T. N.; Melissas, V. S.; Lynch, G. C.; Liu, Y.-P.; Garrett, B. C.; Steckler, R.; Isaacson, A. D.; Rai, S. N.; Hancock, G. C.; Lauderdale, J. G.; Joseph, T.; Truhlar, D. G. *Comput. Phys. Commun.* **1992**, *71*, 235.

(75) Babamov, V. K.; Marcus, R. A. *J. Chem. Phys.* **1981**, *74*, 1790.

(76) Garrett, B. C.; Truhlar, D. G.; Wagner, A. F.; Dunning, T. H., Jr. *J. Chem. Phys.* **1983**, *78*, 4400.

(77) Bondi, D. K.; Connor, J. N. L.; Garrett, B. C.; Truhlar, D. G. *J. Chem. Phys.* **1983**, *78*, 5981.

(78) Garrett, B. C.; Abusalbi, N.; Kouri, D. J.; Truhlar, D. G. *J. Chem. Phys.* **1985**, *83*, 2252.

(79) Liu, L.-P.; Lu, D.-h.; Gonzàlez-Lafont, A.; Truhlar, D. G.; Garrett, B. C. *J. Am. Chem. Soc.* **1993**, *115*, 7806.

(80) Ishida, T.; Schatz, G. C. *Chem. Phys. Lett.* **1999**, *314*, 369.

(81) Collins, M. A.; *Theor. Chem. Acc.* **2002**, *108*, 313.

(82) Tishchenko, O.; Truhlar, D. G., to be published.

(83) Garrett, B. C.; Truhlar, D. G. *J. Phys. Chem.* **1979**, *83*, 1079. Garrett, B. C.; Truhlar, D. G. *Proc. Natl. Acad. Sci. U.S.A.* **1979**, *76*, 4755.

(84) Garrett, B. C.; Truhlar, D. G.; Grev, R. S.; Magnuson, A. W. *J. Phys. Chem.* **1980**, *84*, 1730.

(85) Truhlar, D. G.; Garrett, B. C.; Klippenstein, S. J. *J. Phys. Chem.* **1996**, *100*, 12771.

(86) Fernandez-Ramos, A.; Ellingson, B. A.; Garret, B. C.; Truhlar, D. G. *Rev. Comput. Chem.* In press.

(87) Warshel, A.; Levitt, M. *J. Mol. Biol.* **1976**, *103*, 227.

(88) Singh, U. C.; Kollmann, P. A. *J. Comput. Chem.* **1986**, *7*, 718.

(89) Field, M. J.; Bash, P. A.; Karplus, M. *J. Comput. Chem.* **1990**, *11*, 700.

(90) Thery, V.; Rinaldi, D.; Rivail, J.-L.; Maigret, B.; Ferenczy, G. G. *J. Comput. Chem.* **1994**, *15*, 269.

(91) Stanton, R. V.; Hartsough, D. S.; Merz, K. M., Jr. *J. Comput. Chem.* **1995**, *16*, 113.

(92) Maseras, F.; Morokuma, K. *J. Comput. Chem.* **1995**, *16*, 1170.

(93) Thompson, M. A. *J. Phys. Chem.* **1995**, *99*, 4794.

(94) Barnes, J. A.; Williams, I. H. *Biochem. Soc. Trans.* **1996**, *24*, 263.

(95) Kerdcharoen, T.; Liedl, K. R.; Rode, B. M. *Chem. Phys.* **1996**, *211*, 313.

(96) Assfeld, X.; Rivail, J.-L. *Chem. Phys. Lett.* **1996**, *263*, 100.

(97) Eurenius, K. P.; Chatfield, D. C.; Brooks, B. R.; Hodoscek, M. *Int. J. Quantum. Chem.* **1996**, *60*, 1189.

(98) Bersuker, I. B.; Leong, M. K.; Boggs, J. E.; Pearlman, R. S. *Int. J. Quantum. Chem.* **1997**, *63*, 1051.

(99) Humbel, S.; Sieber, S.; Morokuma, K. *J. Chem. Phys.* **1996**, *105*, 1959.

(100) Day, P. N.; Jensen, J. H.; Gordon, M. S.; Webb, S. P.; Stevens, W. J.; Krauss, M.; Garmer, D.; Basch, H.; Cohen, D. *J. Chem. Phys.* **1996**, *105*, 1968.

(101) Eichler, U.; Kölmel, C. M.; Sauer, J. *J. Comput. Chem.* **1996**, *18*, 463.

(102) Svensson, M.; Humbel, S.; Froese, R. D. J.; Matsubara, T.; Sieber, S.; Morokuma, K. *J. Phys. Chem.* **1996**, *100*, 19357.

(103) Bakowies, D.; Thiel, W. *J. Phys. Chem.* **1996**, *100*, 10580.

(104) Gao, J. *Rev. Comput. Chem.* **1996**, *7*, 119.

(105) Cummins, P. L.; Gready, J. E. *J. Comput. Chem.* **1997**, *18*, 1496.

(106) Sinclair, P. E.; de Vries, A.; Sherwood, P.; Catlow, C. R. A.; van Santen, R. A. *J. Chem. Soc., Faraday Trans.* **1998**, *94*, 3401. Sherwood, P.; De Vries, A. H.; Collins, S. J.; Greatbanks, S. P.; Burton, N. A.; Vincent, M. A.; Hillier, I. H. *Faraday Discuss.* **1997**, *106*, 79.

(107) Burton, N. A.; Harrison, M. J.; Hart, J. C.; Hillier, I. H.; Shepppard, D. W. *Faraday Discuss. Chem. Soc.* **1998**, *110*, 463.

(108) Kaminski, G. A.; Jorgensen, W. L. *J. Phys. Chem. B* **1998**, *102*, 1787.

(109) Gao, J.; Amara, P.; Alhambra, C.; Field, M. J. *J. Phys. Chem. A* **1998**, *102*, 4714.

(110) Tongraar, A.; Liedl, K. R.; Rode, B. M. *J. Phys. Chem. A* **1998**, *102*, 10340.

(111) Woo, T. K.; Cavallo, L.; Ziegler, T. *Theor. Chem. Acc.* **1998**, *100*, 307.

(112) Monard, G.; Merz, K. M., Jr. *Acc. Chem. Res.* **1999**, *32*, 904.

(113) Eichinger, M.; Tavan, P.; Hutter, J.; Parrinello, M. *J. Chem. Phys.* **1999**, *110*, 10452.

(114) Zhang, Y.; Lee, T.-S.; Yang, W. *J. Chem. Phys.* **1999**, *110*, 46.

(115) Philipp, D. M.; Friesner, R. A. *J. Comput. Chem.* **1999**, *20*, 1468.

(116) Shoemaker, J. R.; Burggraf, L. W.; Gordon, M. S. *J. Phys. Chem. A* **1999**, *103*, 3245.

(117) Lyne, P. D.; Hodoscek, M.; Karplus, M. *J. Phys. Chem. A* **1999**, *103*, 3462.

(118) Antes, I.; Thiel, W. *J. Phys. Chem. A* **1999**, *103*, 9290.

(119) Turner, A. J.; Moliner, V.; Williams, I. H. *Phys. Chem. Chem. Phys.* **1999**, *1*, 1323.

(120) Dapprich, S.; Komiromi, I.; Byun, K. S.; Morokuma, K.; Frisch, M. J. *THEOCHEM* **1999**, *461−462*, 1.

(121) Hillier, I. H. *THEOCHEM* **1999**, *463*, 45.

(122) Röthlisberger, U.; Carloni, P.; Doclo, K.; Parrinello, M. *J. Biol. Inorg. Chem.* **2000**, *5*, 236.

(123) Sierka, M.; Sauer, J. *J. Chem. Phys.* **2000**, *112*, 6983.

(124) Reuter, N.; Dejaegere, A.; Maigret, B.; Karplus, M. *J. Phys. Chem. A* **2000**, *104*, 1720.

(125) Kairys, V.; Jensen, J. H. *J. Phys. Chem. A* **2000**, *104*, 6656.

(126) Sushko, P. V.; Shluger, A. L.; Catlow, C. R. A. *Surf. Sci.* **2000**, *450*, 153.

(127) Vreven, T.; Mennucci, B.; da Silva, C. O.; Morokuma, K.; Tomasi, J. *J. Chem. Phys.* **2001**, *115*, 62.

(128) Poteau, R.; Ortega, I.; Alary, F.; Solis, A. R.; Barthelat, J. C.; Daudey, J. P. *J. Phys. Chem. A* **2001**, *105*, 198.

(129) Cui, Q.; Elstner, M.; Kaxiras, E.; Frauenheim, T.; Karplus, M. *J. Phys. Chem. B* **2001**, *105*, 569.

(130) Truhlar, D. G.; Gao, J.; Alhambra, C.; Garcia-Viloca, M.; Corchado, J.; Sanchez, M. L.; Villa, J. *Acc. Chem. Res.* **2002**, *35*, 341.

(131) Gao, J.; Truhlar, D. G. *Annu. Rev. Phys. Chem.* **2002**, *53*, 467.

(132) Kerdcharoen, T.; Morokuma, K. *Chem. Phys. Lett.* **2002**, *355*, 257.

(133) DiLabio, G. A.; Hurley, M. M.; Christiansen, P. A. *J. Chem. Phys.* **2002**, *116*, 9578.

(134) Das, D.; Eurenius, K. P.; Billings, E. M.; Sherwood, P.; Chatfield, D. C.; Hodoscek, M.; Brooks, B. R. *J. Chem. Phys.* **2002**, *117*, 10534.

(135) Mordasini, T.; Curioni, A.; Andreoni, W. *J. Biol. Chem.* **2003**, *278*, 4381.

(136) Kongsted, J.; Osted, A.; Mikkelsen, K. V.; Christiansen, O. *J. Phys. Chem. A* **2003**, *107*, 2578.

(137) Sherwood, P.; de Vries, A. H.; Guest, M. F.; Schreckenbach, G.; Catlow, C. R. A.; French, S. A.; Sokol, A. A.; Bromley, S. T.; Thiel, W.; Turner, A. J.; Billeter, S.; Terstegen, F.; Thiel, S.; Kendrick, J.; Rogers, S. C.; Casci, J.; Watson, M.; King, F.; Karlsen, E.; Sjovoll, M.; Fahmi, A.; Schafer, A.; Lennartz, C. *THEOCHEM* **2003**, *632*, 1.

(138) Amara, P.; Field, M. J. *Theor. Chem. Acc.* **2003**, *109*, 43.

(139) Vreven, T.; Morokuma, K.; Farkas, O.; Schlegel, H. B.; Frisch, M. J. *J. Comput. Chem.* **2003**, *24*, 760.

(140) Pu, J.; Gao, J.; Truhlar, D. G. *J. Phys. Chem. A* **2004**, *108*, 632.

(141) Riccardi, D.; Li, G. H.; Cui, Q. *J. Phys. Chem. B* **2004**, *108*, 6467.

(142) Nam, K.; Gao, J.; York, D. M. *J. Chem. Theory Comput.* **2005**, *1*, 2.

(143) Lin, H.; Truhlar, D. G. *J. Phys. Chem. A* **2005**, *109*, 3991.

(144) Lin, H.; Truhlar, D. G. *Theor. Chem. Acc.* **2006**, in press.

(145) Heyden, A.; Truhlar, D. G. To be published.

(146) Atkinson, R.; Arey, J. *Acc. Chem. Res.* **1998**, *31*, 574.

(147) Reissell, A.; Arey, J.; Atkinson, R. *Int. J. Chem. Kinet.* **2001**, *33*, 56.

(148) Atkinson, R.; Arey, J. *Atmos. Environ.* **2003**, *37*, 1997.

(149) Truhlar D. G., Garret, B. C. *Annu. Rev. Phys. Chem.* **1984**, *35*, 139.

(150) Allison T. C.; Truhlar D. G. In *Modern Methods for Multidimensional Dynamics Computations in Chemistry*; Thompson, D. L., Ed.; World Scientific: Singapore, 1998; p 618.

(151) Pu, J.; Truhlar, D. G. *J. Chem. Phys.* **2002**, *117*, 1479.

(152) Marcus, R. A. *J. Chem. Phys.* **1966**, *45*, 4493.

(153) Wyatt, R. E. *J. Chem. Phys.* **1969**, *51*, 3489.

(154) Duff, J. W.; Truhlar, D. G. *J. Chem. Phys.* **1975**, *52*, 2744.

(155) Miller, W. H.; Handy, N. C.; Adams, J. E. *J. Chem. Phys.* **1980**, *72*, 99.

(156) Lynch, B. J.; Fast, P. L.; Harris, M.; Truhlar, D. G. *J. Phys. Chem. A* **2000**, *104*, 4811.

(157) Lynch, B. J.; Zhao, Y.; Truhlar, D. G. *J. Phys. Chem. A* **2003**, *107*, 1384.

(158) Adamo, C.; Barone, V. *J. Chem. Phys.* **1998**, *108*, 664.

(159) Perdew, J. P. In *Proceedings of the 21st Annual International Symposium on the Electronic Structure of Solids*; Ziesche, P., Eschrig, H., Eds.; Akademie Verlag: Berlin, 1991.

(160) Hehre, W. J.; Radom, L.; Schleyer, P. v. R.; Pople, J. A. *Ab Initio Molecular Orbital Theory*; Wiley: New York, 1986.

(161) Zhao, Y.; Truhlar, D. G. *J. Phys. Chem. A* **2004**, *108*, 6908.

(162) Becke, A. D. *J. Chem. Phys.* **1996**, *104*, 1040.

(163) Frisch, M. J. et al. *Gaussian03*; Gaussian, Inc.: Pittsburgh, PA, 2003.

(164) Ponder, J. W. *TINKER; Version 4.2;* Washington University: St. Louis, MO, 2004.

(165) Besler, B. H.; Merz, K. M., Jr.; Kollman, P. A. *J. Comput. Chem.* **1990**, *11*, 431.

(166) Albu, T. V.; Corchado, J. C.; Kim, Y.; Villà, J.; Xing, J.; Lin, H.; Truhlar, D. G. *MC-TINKER-version 1.1*; University of Minnesota: Minneapolis, MN 55455, 2004.

(167) Lin, H.; Truhlar, D. G. *QMMM; Version 1.0*; University of Minneapolis: Minneapolis, 2004.

(168) Schlegel, H. B. *J. Comput. Chem.* **1982**, *3*, 214.

(169) Corchado, J. C.; Chuang, Y.-Y.; Coitiño, E. L.; Truhlar, D. G. *GAUSSRATE; Version 9.1*; University of Minnesota: Minneapolis, MN, 2003.

(170) Page, M.; McIver, J. W., Jr. *J. Chem. Phys.* **1988**, *88*, 922.

(171) Albu, T. V.; Corchado, J. C.; Kim, Y.; Villà, J.; Xing, J.; Lin, H.; Truhlar, D. G. *MC-TINKERATE; Version 9.1*; University of Minnesota: Minneapolis, MN, 2003.

(172) Schöneboom, J. C.; Lin, H.; Reuter, N.; Thiel, W.; Cohen, S.; Ogliaro, F.; Shaik, S. *J. Am. Chem. Soc.* **2002**, *124*, 8142.